

When Witnesses Defend: A Witness Graph Topological Layer for Adversarial Graph Learning

Naheed Anjum Arafat¹, Debabrota Basu², Yulia Gel³, Yuzhou Chen⁴

¹Nanyang Technological University, Singapore

²Univ. Lille, Inria, CNRS, Centrale Lille, UMR 9189 – CRISTAL, F-59000 Lille, France

³Virginia Tech, USA

⁴University of California, Riverside, USA

naheed_anjum@u.nus.edu, debabrota.basu@inria.fr, ygl@vt.edu, yuzhouc@ucr.edu

Abstract

Capitalizing on the intuitive premise that shape characteristics are more robust to perturbations, we bridge adversarial graph learning with the emerging tools from computational topology, namely, persistent homology representations of graphs. We introduce the concept of witness complex to adversarial analysis on graphs, which allows us to focus only on the salient shape characteristics of graphs, yielded by the subset of the most essential nodes (i.e., landmarks), with minimal loss of topological information on the whole graph. The remaining nodes are then used as witnesses, governing which higher-order graph substructures are incorporated into the learning process. Armed with the witness mechanism, we design *Witness Graph Topological Layer (WGTL)*, which systematically integrates both local and global topological graph feature representations, the impact of which is, in turn, automatically controlled by the robust regularized topological loss. Given the attacker’s budget, we derive the important stability guarantees of both local and global topology encodings and the associated robust topological loss. We illustrate the versatility and efficiency of WGTL by its integration with five GNNs and three existing non-topological defense mechanisms. Our extensive experiments across six datasets demonstrate that WGTL boosts the robustness of GNNs across a range of perturbations and against a range of adversarial attacks. Our datasets and source codes are available at <https://github.com/toggled/WGTL>.

1 Introduction

Recent studies have shown that Graph neural networks (GNNs) are vulnerable to adversarial attacks. Small, often unnoticeable perturbations to the input graph might result in substantial degradation of GNN’s performance in downstream tasks (Jin et al. 2021b). In turn, compared to non-graph data, adversarial analysis of graphs still remains largely underexplored (Sun et al. 2022). Hence, systematic assessment of adversarial contagions and consequently development of robust GNN models able to withstand a wide spectrum of malicious attacks are of significant practical importance.

Presently, the three main strategies to defend GNNs against adversarial attacks are graph purification, adversarial training, and adversarial defense based neural architectures (Feng et al. 2019; Günnemann 2022; Mujkanovic et al. 2022). These existing methods largely rely on pairwise relationships in the graph at a node level while ignoring higher-order graph (sub)structures, their multi-scale properties, and interrelation-

ships, which are instrumental for the downstream learning task (Benson et al. 2018; Torres et al. 2021). Relying on pairwise relationships also results in the removal of a considerable amount of the edges that are actually clean edges, which decreases the gain in robustness (In et al. 2024).

In turn, in the last few years, we have observed a spike of interest in the synergy of graph learning and Persistent Homology (PH) representations of graphs (Zhao and Wang 2019; Carrière et al. 2020; Horn et al. 2022; Yan et al. 2022; Chen, O’Bray, and Borgwardt 2022; Chen and Gel 2023). PH representations enable us to glean intrinsic information about the inherent object shape. By shape here, we broadly understand properties that are invariant under continuous transformations such as twisting, bending, and stretching. This phenomenon can be explained by the important higher-order information, which PH-based shape descriptors deliver about the underlying graph-structured data. This leads to an enhanced GNN performance in a variety of downstream tasks, such as link prediction, and node and graph classification (Hofer et al. 2020; Carrière et al. 2020; Yan et al. 2021; Horn et al. 2022; Chen, Sizikova, and Gel 2022). Furthermore, in view of the invariance with respect to continuous transformations, intuitively we can expect that shape characteristics are to yield higher robustness to random perturbations and adversarial attacks. While this intuitive premise of robustness and its relationship with DNN architectures has been confirmed by some recent studies (Chen, Coskunuzer, and Gel 2021; Gebhart, Schrater, and Hylton 2019; Goibert, Ricatte, and Dohmatob 2022), to the best of our knowledge, there are no attempts to incorporate PH-based graph representations for adversarial defense.

In this paper, we bridge this gap by merging adversarial graph learning with PH representations of graph-structured data. Our key idea is to leverage the concept of witness complex for graph learning. This allows us firstly, to enhance the computational efficiency of the proposed topological defense, which is one of the primary bottlenecks for the wider adoption of topological methods, and lastly, to reduce the impact of less important or noisy graph information. In particular, the goal of the witness complex is to accurately estimate the intrinsic shape properties of the graph using not all available graph information, but *only* a subset of the most representative nodes, called *landmarks*. The remaining nodes are then used as *witnesses*, governing which higher-order graph

substructures shall be incorporated into the process of extracting shape characteristics and the associated graph learning task. This mechanism naturally results in two main benefits. First, it allows us to drastically reduce the computational costs. Second, it allows us to extract salient shape characteristics (i.e., skeleton shape). Our topological defense takes the form of the *Witness Graph Topological Layer (WGTL)* with three novel components: *local and global witness complex-based topological encoding*, *topology prior aggregation*, and *robustness-inducing topological loss*.

The *local witness complex-based features* encapsulate graph topology within the local node neighborhoods, while the *global witness complex-based features* describe global graph topology. Using only local topology prior to the loss function might be vulnerable to local attacks, while only global topology prior might be more susceptible to global attacks. To defend against both types of attacks, both local and global topology prior needs to be combined, thus motivating the design of the topology prior aggregator. Inspired by studies such as Hu et al. (2019); Carriere et al. (2021), we use the robust topological loss as a regularizer to a supervised loss for adversarially robust node representation learning. This allows for control over which shape features are to be included in the defense mechanism.

Our Contributions. Our contributions are summarized as follows:

- We propose the first approach which systematically bridges adversarial graph learning with persistent homology representations of graphs.
- We introduce a novel topological adversarial defense for graph learning, i.e. the *Witness Graph Topological Layer (WGTL)*, based on the notion of the witness complex. WGTL systematically integrates both local and global higher-order graph characteristics. Witness complex enables us to focus only on the salient shape characteristics delivered by the landmark nodes, thereby reducing the computational costs and minimizing the impact of noisy graph information.
- We derive the stability guarantees of both local and global topology encodings and the robust topological loss, given an attacker’s budget. These guarantees show that local and global encodings are stable to external perturbations, while the stability depends on the goodness of the witness complex construction.
- Our extensive experiments spanning six datasets and eight GNNs indicate that WGTL boosts the robustness capabilities of GNNs across a wide range of local and global adversarial attacks, resulting in relative gains up to 18%. WGTL also smoothly integrates with other existing defenses, such as Pro-GNN, GNNGuard, and SimP-GCN improving the relative performance up to 4.95%, 15.67%, and 5.7% respectively. In addition, WGTL is effective on large-scale and heterophilic graphs, as well as against adaptive and node-feature attacks.

1.1 Related Works: Defenses for GNNs

There are broadly three types of defenses: graph purification-based, adversarially robust training, and adversarially robust

architecture (Günemann 2022).

Notable defenses that purify the input graph include SG-GSR (In et al. 2024), Pro-GNN (Jin et al. 2020) and SVD-GCN (Entezari et al. 2020). These methods learn to remove adversarial edges from the poisoned graph without considering higher-order interactions. In contrast, WGTL primarily focuses on learning the key higher-order graph interactions at both local and global levels and then adaptively assessing their potential defense role via topological regularizer. The local and global topological encodings remain robust despite the false positive edges; as a result, WGTL alleviates the problems associated with false positive edges (In et al. 2024), enhancing the overall resilience against attacks.

The adversarial training-based defense methods augment node features with gradients (Kong et al. 2022), or datasets by generating worst-case perturbations (Xu et al. 2019). The goal is to train with the worst-case adversarial perturbations such that the learned model weights become more robust against worst-case perturbation (Günemann 2022). However, adversarial training can not defend against more severe perturbation than the ones they were trained with.

Better architectures such as VAE (Zhang and Ma 2020), Bayesian uncertainty quantification (Feng, Wang, and Ding 2021), and Attention (Zhu et al. 2019; Tang et al. 2020) have also been proposed for adversarial defense. However, none of these tools have explored the use of robust, higher-order graph topological features as prior knowledge for improved defense. Recently, Gabrielsson et al. (2020) designed a topology-driven attack on images and topological loss, but this approach neither considers graph data nor adversarial defense. Among the topology-driven defenses, GNN-Guard (Zhang and Zitnik 2020) discusses graphlet degree vectors to encode node structural properties such as triangles and betweenness centrality. However, unlike the PH features used in WGTL, the graphlet approach is empirical, without theoretical robustness guarantees. In turn, while the robust loss function has been used before Zügner and Günemann (2019b), topological losses have never been used in conjunction with adversarial defenses. The use of a robust loss function as a regularizer for defense is not new; for instance, Zügner and Günemann (2019b) proposed *robust hinge loss* for defense. However, it is unknown if topological losses (Hu et al. 2019; Gabrielsson et al. 2020) can improve adversarial robustness or not.

2 Background: Graphs, Persistent Homology, Complexes, Adversarial ML

Topology of Graphs. $\mathcal{G} \triangleq (\mathcal{V}, \mathcal{E}, X)$ denotes an attributed graph. \mathcal{V} is a set of N nodes. \mathcal{E} is a set of edges. $X \in \mathbb{R}^{N \times F}$ is a node feature matrix, where each node corresponds to an F dimensional feature. The adjacency matrix of \mathcal{G} is a symmetric matrix $A \in \mathbb{R}^{N \times N}$ such that $A_{uv} \triangleq \omega_{uv}$, i.e., edge weight, if nodes u and v are connected and 0, otherwise. For unweighted graphs, we observe $\omega_{uv} = 1$. Furthermore, D represents the degree matrix of \mathcal{G} , such that $D_{uu} \triangleq \sum_{v \in \mathcal{V}} A_{uv}$ and 0, otherwise.

The central ideas leveraged in this paper are the local and global topology of a graph. The topology of a graph is

defined by corresponding geodesic distance. The geodesic distance $d_G(u, v)$ between a pair of vertices u and $v \in \mathcal{V}$ is defined as the length of the shortest path between u and v . The path length is defined as the sum of weights of the edges connecting the vertices u and v . Endowed with the canonical metric induced by the geodesic distance $d_G : \mathcal{V} \times \mathcal{V} \rightarrow \mathbb{R}^{\geq 0}$, a weighted simple graph \mathcal{G} transforms into a metric space (\mathcal{V}, d_G) . For a given positive real number $\epsilon > 0$, the set of nodes that are no more than geodesic ϵ away from a given node determines the local topology of that node. When $\epsilon = \text{Diam}(\mathcal{G})$, i.e. the diameter of \mathcal{G} , we retrieve the global topology of the graph. Increasing ϵ from 1 to $\text{Diam}(\mathcal{G})$ allows us to retrieve the evolution of the inherent graph features, like connected components, cycles, voids, etc. (Edelsbrunner, Letscher, and Zomorodian 2002; Zomorodian 2005).

Persistent Homology. To retrieve the evolution of graph features, we employ a Persistent Homology-based approach, a machinery rooted in computational topology. Our topological space originates from subgraphs $\{\mathcal{G}_\alpha : \forall (u, v) \in \mathcal{G}_\alpha, d_G(u, v) \leq \alpha\}_{1 \leq \alpha \leq \text{Diam}(\mathcal{G})}$, where every subgraph \mathcal{G}_α contains all edges of length less than α . To incorporate higher-order information, simplicial complexes $\{\mathcal{K}(\mathcal{G}_\alpha)\}_\alpha$ are constructed, where a higher-order simplex $\sigma \in \mathcal{K}(\mathcal{G}_\alpha)$ if for every node pair $(u, v) \in \sigma$, the simplex $[uv] \in \mathcal{K}(\mathcal{G}_\alpha)$, in other words $d_G(u, v) \leq \alpha$. This nested sequence of simplicial complexes is called a *filtration*, with α representing the filtration value.

The key idea of PH is to choose multiple scale parameters α and study changes in topological features that occur to \mathcal{G} , which evolves with respect to α . Equipped with the filtration of complexes, we can trace data shape patterns, i.e. the d homology groups, such as independent components, holes, and cavities which appear and merge as scale α changes. For each topological feature ρ , we record the indices b_ρ and d_ρ of $\mathcal{K}(\mathcal{G}_{b_\rho})$ and $\mathcal{K}(\mathcal{G}_{d_\rho})$, where ρ is first and last observed, respectively. We say that a pair (b_ρ, d_ρ) represents the birth and death times of ρ , and $(d_\rho - b_\rho)$ is its corresponding lifespan (or *persistence*). In general, topological features with longer persistence are considered valuable, while features with shorter persistence are often associated with topological noise. The extracted topological information over the filtration $\{\mathcal{K}_{\alpha_j}\}$ is then represented in \mathbb{R}^2 as a *Persistence Diagram (PD)*, such that $\text{PD} = \{(b_\rho, d_\rho) \in \mathbb{R}^2 : d_\rho > b_\rho\} \cup \Delta$. $\Delta = \{(t, t) | t \in \mathbb{R}\}$ is the diagonal set containing points counted with infinite multiplicity. Another useful representation of persistent topological features is *Persistence Image (PI)* that vectorizes the persistence diagram with a Gaussian kernel and a piece-wise linear weighting function (Adams et al. 2017). Persistence images are deployed to make a classifier “topology-aware” and are known to be helpful in graph classification (Zhao and Wang 2019; Rieck et al. 2020).

Witness Complexes. There are multiple ways to construct an abstract simplicial complex \mathcal{K} (Zomorodian 2005). Due to its computational benefits, one of the widely adopted approaches is a *Vietoris-Rips complex (VR)*. However, the VR complex uses the entire observed data to describe the underlying topological space, and thus, does not efficiently scale to large and noisy datasets (Zomorodian 2010). In contrast, a *witness complex* captures the data shapes using only on

a significantly smaller subset $\mathcal{L} \subseteq \mathcal{V}$, called a set of *landmarks* (De Silva and Carlsson 2004). In turn, all other points in \mathcal{V} are used as “witnesses” that govern the appearances of simplices in the witness complex. Arafat, Basu, and Bressan (2020) demonstrate algorithms to construct landmark sets, their computational efficiencies, and stability of the induced *witness complex*. We leverage witness complex to scale to large graph datasets.

Definition 2.1 (Weak Witness Complex (De Silva and Carlsson 2004)). We call $w \in \mathcal{V}$ to be a *weak witness* for a simplex $\sigma = [v_0 v_1 \dots v_l]$, where $v_i \in \mathcal{V}$ for $i = 0, 1, \dots, l$ and $l \in \mathbb{N}$, with respect to \mathcal{L} if and only if $d_G(w, v) \leq d_G(w, u)$ for all $v \in \sigma$ and $u \in \mathcal{L} \setminus \sigma$. The *weak witness complex* $\text{Wit}(\mathcal{L}, \mathcal{G})$ of the graph \mathcal{G} with respect to the landmark set \mathcal{L} has a node set formed by the landmark points in \mathcal{L} , and a subset σ of \mathcal{L} is in $\text{Wit}(\mathcal{L}, \mathcal{G})$ if and only if there exists a corresponding weak witness in the graph \mathcal{G} .

Adversarial ML and Robust Representations. Graph Neural Networks (GNNs) aim to learn a labelling function that looks into the features the nodes in the graph \mathcal{G} and assign one of the C labels $y_v \in \{1, \dots, C\}$ to each node $v \in \mathcal{V}$ (Kipf and Welling 2016). In order to learn to labelling, GNNs often learn compact, low-dimensional representations, aka *embeddings* $R : \mathcal{G} \times \mathcal{V} \rightarrow \mathbb{R}^r$, for nodes that capture the structure of the nodes’ neighbourhoods and their features, and then apply a classification rule $f : \mathbb{R}^r \rightarrow \{1, \dots, C\}$ on the embedding (Kipf and Welling 2016; Hamilton, Ying, and Leskovec 2017; Zhang and Zitnik 2020).

The goal of a robust GNN training mechanism is to learn a labelling function $f \circ R$ such that the change in the predicted labels, i.e. $|(f \circ R)(\mathcal{G}') - (f \circ R)(\mathcal{G})|$, is the minimum, when a graph \mathcal{G} is adversarially perturbed to become \mathcal{G}' (Zhang and Zitnik 2020). The budget of perturbation is defined by $\delta = \|\mathcal{G} - \mathcal{G}'\|_p$. p is often fixed to 0 or 1 (Xu et al. 2019; Wu et al. 2019b; Zügner and Günnemann 2019b). There are different ways to design a robust training mechanism, such as training with an adversarially robust loss function (Xu et al. 2019), using a stabilising regularizer to the classification loss (Zügner and Günnemann 2019b), learning a robust representation of the graph (Engstrom et al. 2019; Liu et al. 2023), etc.

In this paper, we aim to design a *robust representation* R of the graph \mathcal{G} using its persistent homologies. Specifically, we call a graph representation R *robust*, if for $p, q > 0$,

$$\|R(\mathcal{G}) - R(\mathcal{G}')\|_p = \mathcal{O}(\delta), \text{ when } \|\mathcal{G} - \mathcal{G}'\|_q = \delta.$$

In the following section, we propose WGTL, which is a topology-aware graph representation, and show that WGTL achieves this robust representation property.

3 Learning a Robust Topology-aware Graph Representation

The general idea is that encoding robust graph structural features as prior knowledge to a graph representation learning framework should induce a degree of robustness against adversarial attacks. Graph measures that capture global properties of the graph and measures that rely on aggregated statistics are known to be robust against small perturbations.

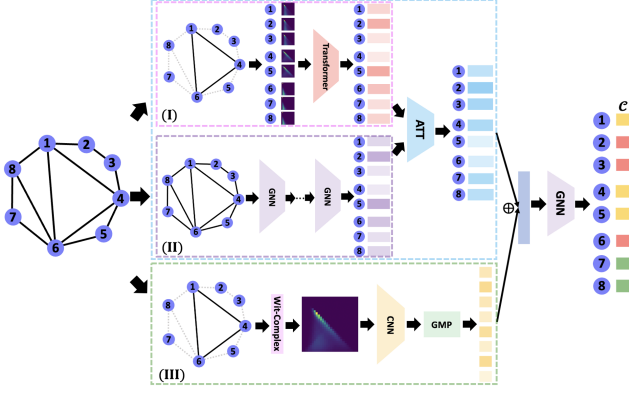


Figure 1: Architecture of Witness Graph Topological Layer.

Examples include degree distribution, clustering coefficients, average path length, diameter, largest eigenvalue and the corresponding eigenvector, and certain centrality measures, e.g., betweenness and closeness centralities. However, these measures are not multiscale in nature. Therefore, they fail to encapsulate global graph structure at multiple levels of granularity. Many of them, e.g., degree distribution, and clustering coefficients, only encode 1-hop or 2-hop information. Such information can be learned by a shallow GNN through message passing, rendering such features less useful as a prior. Features such as average path length and diameter are too coarse-scale (scalar-valued) and do not help a GNN to discern the nodes. Since existing robust graph features can not encode both local and global topological information at multiple scales, we introduce local and global topology encodings based on persistent homology as representations to the GNNs (Section 3.1). We also propose to use a topological loss as a regularizer to learn topological features better (Section 3.2).

3.1 Witness Graph Topological Layer

Now, we describe the architecture of the Witness Graph Topological Layer (WGTL) (Figure 1).

Component I: Local Topology Encoding. *Local topology encoding* component of WGTL (Figure 1) computes local topological features of every node in three steps. First, we choose a landmark set \mathcal{L} from the input graph \mathcal{G} . An important hyperparameter of the local topology encoding is the choice of the number of landmarks. Choosing too few landmarks would reduce the informativeness of the latent embedding. Choosing too many landmarks (i.e., $|\mathcal{V}|$), on top of being computationally expensive, might be redundant because the topological features of a neighboring node are likely to be the same. Secondly, we use the landmarks to construct an ϵ -net of \mathcal{G} (Arafat, Basu, and Bressan 2020), i.e. a set of subgraphs $\{\mathcal{G}_l^\epsilon\}_{l \in \mathcal{L}}$. Here, $\epsilon \triangleq \max_{l_1, l_2 \in \mathcal{L}} 0.5d_{\mathcal{G}}(l_1, l_2)$. We compute witness complex for each of these \mathcal{G}_l^ϵ 's, and the corresponding persistence images $\text{PI}(\text{Wit}(\mathcal{G}_l^\epsilon))$. Finally, we attribute the PIs of the landmarks to each node in its ϵ -cover and pass them through a vision transformer model to compute the local topology encoding, i.e. $\mathbf{Z}_{TL} = \text{Transformer}(\text{PI}(\text{Wit}(\mathcal{G}^\epsilon))_1, \dots, \text{PI}(\text{Wit}(\mathcal{G}^\epsilon))_N)$. The local topology encoding \mathbf{Z}_{TL} is a latent embedding of local

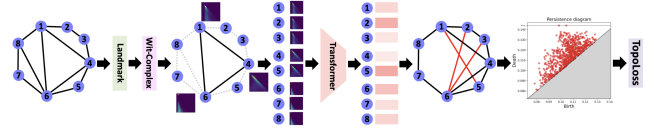


Figure 2: Illustration of Witness Complex-based topological regularizer L_{Topo} .

topological features of each node in \mathcal{G} .

When the attack model poisons the adjacency matrix, especially in the cases of global attacks, the local topological encodings are also implicitly perturbed. In Theorem 3.1, we show that local topological encodings are stable w.r.t. perturbations in the input graph. Specifically, if an attacker's budget is $\mathcal{O}(\delta)$, the encoded local topology is perturbed by $\mathcal{O}(C_\epsilon(\delta + \epsilon))$. The bound indicates the trade-off due to landmark selection. If we select fewer landmarks, computation becomes faster and we encode topological features of a larger neighborhood. However, an increase in C_ϵ yields less stable encoding. Whereas if we select more landmarks, we get more stable encoding but we lose informativeness of the local region and computational efficiency.

Theorem 3.1 (Stability of the encoded local topology). *Let us denote the persistence diagram obtained from local topology encoding of \mathcal{G} as $\text{T}(\mathcal{G})$ (Figure 2). For any $p < \infty$ and C_ϵ being the maximum cardinality of the ϵ -neighborhood created by the landmarks, we obtain that for any graph perturbation $\|\mathcal{G} - \mathcal{G}'\|_1 = \mathcal{O}(\delta)$ the final persistence diagram representation changes by $W_p(\text{T}(\mathcal{G}), \text{T}(\mathcal{G}')) = \mathcal{O}(C_\epsilon \delta)$, if we have access to Čech simplicial complexes, and $W_p(\text{T}(\mathcal{G}), \text{T}(\mathcal{G}')) = \mathcal{O}(C_\epsilon(\delta + \epsilon))$, if Witness complex is used for the Local Persistence Images.*

Component II: Graph Representation Learning. The component II of WGTL deploys in cascade M GNN layers with ReLU activation function and weights $\{\Theta^{(m)}\}_{m=1}^M$. The representation learned at the m -th layer is given by $\mathbf{Z}_G^{(m+1)} = \text{ReLU}(\tilde{\mathbf{D}}^{-\frac{1}{2}} \tilde{\mathbf{A}} \tilde{\mathbf{D}}^{\frac{1}{2}} \mathbf{Z}_G^{(m)} \Theta^{(m)})$. Here, $\mathbf{Z}_G^{(0)} = \mathcal{G}$, $\tilde{\mathbf{A}} = \mathbf{A} + \mathbf{I}$, and $\tilde{\mathbf{D}}$ is the corresponding degree matrix.

Component III: Global Topology Encoding. The *global topological encoding* represents the global witness complex-based topological features of a graph (Component III in Figure 1). First, we use the input adjacency matrix to compute the lengths of all-pair shortest paths (geodesics) among the nodes. The topological space represented by the geodesic distance matrix is used to compute the global witness complex-based persistence image $\text{PI}(\text{Wit}(\mathcal{G}))$ of the graph (Arafat, Basu, and Bressan 2020). Finally, the persistence image representation is encoded by a Convolutional Neural Network (CNN)-based model to obtain the *global topological encoding* $\mathbf{Z}_{TG} \triangleq \xi_{\max}(\text{CNN}(\text{PI}(\text{Wit}(\mathcal{G}))))$. Here, $\xi_{\max}(\cdot)$ denotes global max-pooling operation. The global topology encoding encapsulates the global topological features, such as the equivalent class of connected nodes, cycles, and voids in the graph.

The stability of global persistence diagram representation is a well-known classical result in persistence homology (Cohen-Steiner, Edelsbrunner, and Harer 2005; Chazal et al. 2008). However, given an attacker's budget of δ , the

stability of the encoded global topology is an important result for the practical purposes of this paper. Theorem 3.2 shows that under a $\mathcal{O}(\delta)$ perturbation of the input graph, the global topology encoding is perturbed by $\mathcal{O}(\delta + \epsilon)$. Hence, the global topological encoding inherits the robustness property of persistent homology and induces robust learning under adversarial attacks.

Proposition 3.2 (Stability of the encoded global topology). *If the landmarks selected for the witness complex induce an ϵ -net of the graph with $\epsilon > 0$, we obtain that for any graph perturbation $\|\mathcal{G} - \mathcal{G}'\|_1 = \mathcal{O}(\delta)$ the global persistence image representation changes by $\|\text{PI}(\text{Wit}^{\text{glob}}(\mathcal{G})) - \text{PI}(\text{Wit}^{\text{glob}}(\mathcal{G}'))\|_\infty = \mathcal{O}(\delta + \epsilon)$, and it reduces to $\mathcal{O}(\delta)$, if we have access to the Čech simplicial complexes for \mathcal{G} .*

WGTL: Aggregating Global and Local Encodings. We can aggregate the local and global topology encodings with the latent embedding of graph convolution layers in different ways. Figure 1 shows the approach that empirically provides the most effective defense against adversarial attacks.

The aggregation of the three encodings is computed in two steps. First, to adaptively learn the intrinsic dependencies between learned node embedding and latent local topological encodings, we utilize the attention mechanism to focus on the importance of task-relevant components in the learned representations, i.e. $(\alpha_G, \alpha_{T_L}) \triangleq \text{Att}(\mathbf{Z}_H, \mathbf{Z}_{T_L})$. In practice, we compute attention coefficients as $\alpha_i = \text{softmax}_i(\Upsilon_{\text{Att}} \tanh(\Xi \mathbf{Z}_i))$, where $\Upsilon_{\text{Att}} \in \mathbb{R}^{1 \times d_{\text{out}}}$ is a linear transformation, Ξ is the trainable weight matrix, and the softmax function is used to normalize the attention vector. Then, we obtain the final embedding by combining two embeddings $\mathbf{Z}_{\text{AGG}} = \alpha_G \times \mathbf{Z}_G + \alpha_{T_L} \times \mathbf{Z}_{T_L}$. Finally, we combine the learned embedding \mathbf{Z}_{AGG} with the latent global topological representation \mathbf{Z}_{T_G} , such that $\mathbf{Z}_{\text{WGTL}} = \mathbf{Z}_{\text{AGG}} \mathbf{Z}_{T_G}$. The node representation \mathbf{Z}_{WGTL} encapsulates both global and local topology priors. We call \mathbf{Z}_{WGTL} the *aggregated topological priors*. We feed \mathbf{Z}_{WGTL} into a graph convolutional layer and use a differentiable classifier (here we use a softmax layer) to make node classification. In the following, we show the stability of the aggregated topological priors.

Proposition 3.3 (Stability of the aggregated topological encoding). *If the landmarks selected for the witness complex induce an ϵ -net of the graph with $\epsilon > 0$ and L_{GNN} is the Lipschitz constant of the GNNs in Component II, then for a perturbation $\|\mathcal{G} - \mathcal{G}'\|_1 = \mathcal{O}(\delta)$, the encoding \mathbf{Z}_{WGTL} changes by*

$$\|\mathbf{Z}_{\text{WGTL}}(\mathcal{G}) - \mathbf{Z}_{\text{WGTL}}(\mathcal{G}')\|_1 = \mathcal{O}((C_\epsilon + L_{\text{GNN}})(\delta + \epsilon)^2).$$

Proposition 3.3 shows that the final representations computed by WGTL is stable under adversarial attacks. The stability depends on the approximation trade-off induced by the landmark set and the Lipschitz stability of the GNN layers (Jia et al. 2023).

3.2 Topological Loss as a Regularizer

In Section 3.1, we propose using the aggregated topology encodings to predict node labels for downstream node classification tasks through a GNN backbone. In this case, we use a supervised loss L_{supv} that facilitate learning the aggregated

topology priors for classification. We empirically observe that our topology encoding already provides a certain degree of robustness (see ablation studies in Appendix D).

However, the supervised loss function only explicitly enforces misclassification constraints on the defense model. It does not explicitly enforce any topological constraint such that the topological encodings themselves iteratively become more robust while training. Hence, for increased robustness, we propose to use topological loss L_{topo} that explicitly encodes the birth and death of the topological features in the auxiliary graph (ref. Figure 2) reconstructed from the transformer output. Specifically,

$$L_{\text{topo},k}(\mathbf{T}(\mathcal{G})) \triangleq \sum_{i=1}^m (d_i - b_i)^p \left(\frac{d_i + b_i}{2} \right)^q, \quad (1)$$

where m is the number of points in the persistence diagram of the auxiliary graph reconstructed from the transformer output and $k = \max\{p, q\}$. In practice, we use $k = 2$. Use of such topological loss was first proposed for image segmentation (Hu et al. 2019). Gabrielson et al. (2020) uses it as a regularizer in designing GAN and adversarial attacks on images. In contrast, we use it to induce stability in the encoding and to defend against adversarial attacks. The benefits of using the topological loss are two-fold:

- (i) **Persistent and Stable Feature Selection:** Minimising $L_{\text{topo},k}$ causes removal of topological features with smaller persistence, i.e., $(d_i - b_i)$. As such, the regularizer acts as a sparsity-inducing feature selector. By minimizing L_{topo} , we are training to learn latent representation such that only the most persistent features remain in the encoded local topology. Such features are known to be more stable and represent more robust structures of the graph.
- (ii) **Robustness to Local Perturbations:** A localized attack perturbing certain nodes or edges is expected to appear as topological noise in the final persistent diagram, and should exhibit lower persistence. Since minimizing L_{topo} forces the local topology encodings to eliminate features with small persistences, using L_{topo} as a regularizer with L_{supv} induces robustness to local perturbations in final classification tasks.

Proposition 3.4 quantifies the stability of the topological regularizer $L_{\text{topo},k}$ under any attack with perturbation budget $\mathcal{O}(\delta)$. Specifically, it shows that the stability depends on a trade-off between the maximum persistence of the final graph representation, $A_\Phi(\mathcal{G})$, in Figure 2, and the number of non-zero persistent features in the final encoding. Hence, it reflects our discussion above.

Proposition 3.4 (Stability of L_{topo}). *Let us assume that the cardinality of any ϵ -neighborhood of \mathcal{G} grows polynomially, i.e. $C_\epsilon = \mathcal{O}(\epsilon^{-M})$ for an $M > 0$. If m is the number of points in the persistence diagram, $2k = 2 \max\{p, q\} > M$, and $A(\mathcal{G})$ is the auxiliary graph constructed from the local topology encodings (Fig. 2), $L_{\text{topo},k}(\mathbf{T}(\mathcal{G}))$ is stable w.r.t. a perturbation of \mathcal{G} , i.e. $\|\mathcal{G} - \mathcal{G}'\|_1 = \delta$.*

$$\begin{aligned} & |L_{\text{topo},k}(\mathbf{T}(\mathcal{G})) - L_{\text{topo},k}(\mathbf{T}(\mathcal{G}'))| \\ &= \mathcal{O}((\epsilon^{-4kM} \text{Diam}(A(\mathcal{G})) + m\epsilon^{-2k} \text{Diam}(\mathcal{G})^{2k}) \delta). \end{aligned}$$

Dataset	#nodes (LCC)	#edges (LCC)	#classes	#features
Cora-ML	2,485	5,069	7	1,433
Citeseer	2,110	3,668	6	3,703
Pubmed	19,717	44,338	3	500
Polblogs	1,222	16,714	2	None
OGBN-arXiv	169,343	1,157,799	40	128
Snap-patents	4562	12103	5	269

Table 1: Dataset statistics: only the largest connected component (LCC) is considered.

4 Experimental Evaluation

We evaluate the proposed WGTL on the node classification task for clean and attacked graphs across a range of perturbation rates. We validate the proposed approach on six benchmark datasets: Citeseer, Cora, Pubmed, Polblogs, OGBN-Arxiv, and Snap-patents (ref. Table 1). *We report the mean and standard deviation of accuracies over 10 runs. The best performance is highlighted in bold while the best result on a dataset for a given perturbation rate is indicated by *.* Note that, throughout our experiments, we use 0-dimensional topological features. All the hyperparameters are chosen by performing cross-validation.

We defer the dataset descriptions, implementation details, ablation studies, impact of the #landmarks on performance, comparison with Vietoris-Rips, and additional experimental results such as handling node features, heterophilic graphs, adaptive attacks, and the adoption of other topological vectorization methods in WGTL to the Appendix.

Landmark Selection for Local and Global Topology Encodings. There are several approaches to selecting landmarks, e.g., random selection (De Silva and Carlsson 2004), max-min selection (De Silva and Carlsson 2004), ϵ -net (Arafat, Basu, and Bressan 2020) based and centrality-based selection (Chen and Gel 2023). In our experiments, we select landmarks based on degree centrality. As shown by Chen and Gel (2023), doing so helps to improve the classification performance. On Cora-ML, Citeseer, and Polblogs, we select 5% nodes, on Pubmed and Snap-patents we select 2% nodes and on OGBN-arXiv we select 0.05% nodes as landmarks to keep #landmarks roughly invariant across datasets.

Adversarial Attacks: Local and Global. We deploy four local and global poisoning attacks, with perturbation rates, i.e., the ratio of changed edges, from 0% to 10%, to evaluate the robustness of WGTL. We consider a fixed GCN without weight re-training as the surrogate for all attacks. As a local attack, we deploy netack (Zügner, Akbarnejad, and Günnemann 2018). *Due to the stability of WGTL and topological regularizer, we expect to be robust to such local attacks.* As global (non-targeted) poisoning attacks, we deploy metattack (Zügner and Günnemann 2019a), and two topological attacks, namely PGD (Xu et al. 2019) and Meta-PGD (Mujkanovic et al. 2022). Metattack treats the graph as a hyperparameter and greedily selects perturbations based on meta-gradient for node pairs until the budget is exhausted. We keep all the default parameter settings (e.g., $\lambda = 0$) following the original implementation (Zügner and Günnemann 2019a). For Cora-ML, Citeseer and Polblogs, we apply the most effective Meta-Self variant, while for Pubmed, we apply

Dataset	Models	Perturbation Rate		
		0%	5%	10%
Cora-ML	Pro-GNN	82.98 \pm 0.23	80.14 \pm 1.34	71.59 \pm 1.33
	Pro-GNN+WGTL	83.85\pm0.38	81.90\pm0.73	72.51\pm0.76
	GCN+GNNGuard	83.21 \pm 0.34	76.57 \pm 0.50	69.13 \pm 0.77
	GCN+GNNGuard+WGTL	*84.78\pm0.43	*83.23\pm0.82	*79.96\pm0.49
	SimP-GCN	79.52 \pm 1.81	74.75 \pm 1.40	70.87 \pm 1.70
	SimP-GCN+WGTL	81.49\pm0.52	76.65\pm0.65	72.88\pm0.83
Citeseer	ProGNN	72.34 \pm 0.99	68.96 \pm 0.67	67.36 \pm 1.12
	ProGNN+WGTL	72.83\pm0.94	71.85\pm0.74	70.70\pm0.57
	GCN+GNNGuard	71.82 \pm 0.43	70.79 \pm 0.22	66.86 \pm 0.54
	GCN+GNNGuard+WGTL	73.37\pm0.63	72.57\pm0.17	66.93\pm0.21
	SimP-GCN	73.73 \pm 1.54	73.06 \pm 2.09	72.51 \pm 1.25
	SimP-GCN+WGTL	*74.32\pm0.19	*74.05\pm0.71	*73.09\pm0.50
Pubmed	Pro-GNN	87.33 \pm 0.18	87.25 \pm 0.09	87.20 \pm 0.12
	Pro-GNN + WGTL (ours)	87.90\pm0.30	*87.77\pm0.08	*87.67\pm0.22
	GCN+GNNGuard	83.63 \pm 0.08	79.02 \pm 0.14	76.58 \pm 0.16
	GCN+GNNGuard+WGTL	OOM	OOM	OOM
	SimP-GCN	*88.11 \pm 0.10	86.98 \pm 0.19	86.30 \pm 0.28
	SimP-GCN+WGTL	OOM	OOM	OOM
Polblogs	GCN+GNNGuard	95.03 \pm 0.25	73.25 \pm 0.16	72.76 \pm 0.75
	GCN+GNNGuard+WGTL	*96.22\pm0.25	*73.62\pm0.22	*73.72\pm1.00
	SimP-GCN	89.78 \pm 6.47	65.75 \pm 5.03	61.53 \pm 6.41
	SimP-GCN+WGTL	94.56\pm0.24	69.78\pm4.10	69.55\pm4.42

Table 2: Comparison of performances (avg. accuracy \pm std.) with existing defenses under metattack.

the approximate variant (A-Meta-Self) to save memory and time (Jin et al. 2020). PGD attack (Xu et al. 2019) adapts the well-known Projected Gradient Descent-based attack in adversarial ML to graphs. Recently, Meta-PGD is proposed (Mujkanovic et al. 2022) by applying PGD on the meta-gradients. It combines the effectiveness of metattack and PGD, and is shown to be the most effective topological attack at present. *Though global attacks are expected to be more challenging while using topological features, we demonstrate that WGTL still yields significant robustness.* Further details on attack implementations and attackers’ budgets are in Appendix B. The results for PGD and Meta-PGD attacks are in Appendix F.

Objectives. *We implemented and compared WGTL with 3 existing defenses and 5 GNN backbones to study five questions. (Q1) Can WGTL enhance the robustness of the existing defenses? (Q2) Can WGTL enhance the robustness of existing backbone graph convolution layers? (Q3) Is WGTL still effective when the topological features are computed on poisoned graphs instead of clean graphs? (Q4) How does WGTL perform on large graphs? (Q5) Is WGTL computationally efficient?*

Q1. Performance of WGTL Defense w.r.t. Existing Defenses. We compare our method with three state-of-the-art defenses: Pro-GNN (Jin et al. 2020), GNNGuard (Zhang and Zitnik 2020), and SimP-GCN (Jin et al. 2021a). Table 2 illustrates the comparative performances on three citation networks under a global attack, i.e. metattack. We observe that our Pro-GNN+WGTL is always better than other baselines on all datasets. Following Jin et al. (2020), we omit Pro-GNN for Polblogs. As a consequence, we gain 0.68% - 4.96% of relative improvements on Cora-ML and Citeseer. Similarly, we observe that GCN+GNNGuard+WGTL outperforms GCN+GNNGuard and SimP-GCN+WGTL outperforms SimP-GCN by 0.10% - 15.67% and 2.4% - 5.7%, respectively, across all datasets. The results reveal that WGTL

Dataset	Model	Perturbation Rate		
		0%	5%	10%
Cora-ML	GCN	82.87±0.83	76.55±0.79	70.39±1.28
	GCN + WGTL (ours)	83.83±0.55	78.63±0.76	73.41±0.82
	ChebNet	80.74±0.42	74.35±1.2	66.62±1.44
	ChebNet + WGTL (ours)	82.96±1.08	76.00±1.22	69.49±0.89
	GAT	84.25±0.67	79.88±1.09	72.63±1.56
	GAT + WGTL (ours)	*86.07±2.10	80.80±0.87	75.80±0.79
Polblogs	GraphSAGE	81.00±0.27	74.81±1.2	70.92±1.18
	GraphSAGE + WGTL (ours)	83.63±0.35	*82.61±0.65	*81.19±1.13
	GCN	94.40±1.47	71.41±2.42	69.16±1.86
	GCN + WGTL (ours)	*95.95±0.15	74.62±0.42	72.84±0.86
	ChebNet	73.10±7.13	67.63±1.71	67.36±0.85
	ChebNet + WGTL (ours)	92.50±1.10	71.17±0.10	68.03±0.87
	GAT	95.28±0.51	75.83±0.90	73.11±1.20
	GAT + WGTL (ours)	95.87±0.26	*83.13±0.32	80.06±0.50
	GraphSAGE	94.52±0.27	77.44 ± 1.71	74.66±0.85
	GraphSAGE + WGTL (ours)	95.58±0.50	82.62±0.65	*81.49±0.86

Table 3: Robustness of various backbone GNNs (avg. accuracy±std.) under metttack

enhances not only model expressiveness but also the robustness of the GNN-based models. The performance comparison under netttack is shown in Table 12 of Appendix F.

Q2. WGTL Enhances Robustness of GNNs. WGTL is flexible in the sense that it can employ existing GNN layers to enhance their robustness. To be precise, we have employed the existing GNN backbones as component II in Figure 1 to enhance their robustness. Since global attacks target global graph topology, global poisoning attacks are supposed to be more challenging for the proposed *topology-based* defense WGTL. Despite that, we observe that WGTL consistently improves the robustness of all backbone GNNs in Table 3. The performance of our method, including that of the backbone GNNs, deteriorates faster on Polblogs than on the other datasets. This is because Polblogs does not have node features, and having informative node features can help GNN differentiate between nodes and learn meaningful representations despite changes in the graph structure. With node features lacking, the Polblogs graph has comparatively less resilience against graph structural perturbations. We discuss the results on Netttack and results with SGC backbone (Wu et al. 2019a) in Appendix F.

Q3. Performance of WGTL on Poisoned Graphs. So far, the local and global topological features are computed on clean graphs assuming that these features can be computed before the attacker poisons the graph. However, such an assumption is restrictive as the attacker might poison the graph at any point before and during training. As a result, the topological features computed by WGTL might also be poisoned, as they were computed based on the poisoned graph. WGTL_P employs poisoned graphs as inputs in the schematics of Figure 1 and 2. We present the performance of WGTL_P on Cora-ML and Polblogs under metttack in Table 4. We observe a consistent improvement over the baseline models across various datasets and perturbation rates. In this setting, we find GAT+WGTL_P and GraphSAGE+WGTL_P to be the best performing models. We observe that *WGTL robustifies the*

Dataset	Models	Perturbation Rate		
		0%	5%	10%
Cora-ML	GCN	82.87±0.83	76.55±0.79	70.39±1.28
	GCN+WGTL _P (ours)	83.83±0.55	76.96±0.76	71.31±0.85
	GAT	84.25±0.67	79.88±1.09	72.63±1.56
	GAT+WGTL _P (ours)	*86.07±2.10	81.43±0.75	*73.74±1.92
	GraphSAGE	81.00±0.27	74.81±1.20	70.92±1.18
	GraphSAGE+WGTL _P (ours)	83.63±0.35	*82.15±1.25	73.57±0.73
	ProGNN	82.98±0.23	80.14±1.34	71.59±1.33
	ProGNN+WGTL _P (ours)	83.85±0.38	81.69±1.83	72.71±1.26
	GCN+GNNGuard	83.21±0.34	76.57±0.50	69.13±0.77
	GCN+GNNGuard+WGTL _P (ours)	84.78±0.43	77.08±0.32	70.15±0.89
	GCN	94.40±1.47	71.41±2.42	69.16±1.86
	GCN+WGTL _P (ours)	95.95±0.15	73.02±1.13	74.52±0.28
Polblogs	GAT	95.28±0.51	75.83±0.90	73.11±1.20
	GAT+WGTL _P (ours)	95.87±0.26	76.05±0.79	74.21±0.74
	GraphSAGE	94.54±0.27	77.44±1.71	74.66±0.85
	GraphSAGE+WGTL _P (ours)	95.58±0.50	*78.65±1.32	*74.93±0.81
	GCN+GNNGuard	95.03±0.25	73.25 ± 0.16	72.76±0.75
	GCN+GNNGuard+WGTL _P (ours)	*96.22±0.25	73.62±0.22	73.72±1.00

Table 4: Performance on poisoned graph (avg. accuracy±std) under metttack.

Models	Perturbation Rate	
	0%	10%
GCN	27.33	21.56
GCN+WGTL _P (ours)	28.32	22.89

Table 5: Performance on OGBN-arXiv under PRBCD attack.

existing backbones, e.g., GAT and SAGE, more compared to all other defenses.

Q4. Performance of WGTL on a large-scale graph. We have applied the PRBCD attack to generate the perturbed OGBN-arXiv graph since we found that other attacks, such as Metttack and Netttack, do not scale to such large-scale graphs (Geisler et al. 2021). Following Geisler et al. (2021), we train a 3-layer GCN to generate attacks. We then present the comparison between GCN and GCN + WGTL_P on non-poisoned (0%) and poisoned (10%) perturbed graphs in Table 5. We observe that the GCN equipped with our WGTL outperforms GCN on both clean and perturbed OGBN-arXiv.

Q5. Computational Complexity and Efficiency of WGTL. Landmark selection (top- $|\mathcal{L}|$ degree nodes) has complexity $\mathcal{O}(N \log(N))$. To compute witness features, we compute (1) landmarks-to-witness distances costing $\mathcal{O}(|\mathcal{L}|(N + |\mathcal{E}|))$ due to BFS-traversal from landmarks, (2) landmark-to-landmark distances costing $\mathcal{O}(|\mathcal{L}|^2)$, and finally (3) persistent homology via boundary matrix construction and reduction (Edelsbrunner, Letscher, and Zomorodian 2002). Matrix reduction algorithm costs $\mathcal{O}(\zeta^3)$, where ζ is the #simplices in a filtration. Overall computational complexity of computing witness topological feature on a graph is $\mathcal{O}(|\mathcal{L}|(N + |\mathcal{E}|) + |\mathcal{L}|^2 + \zeta^3)$.

Table 6 shows the total CPU-time to compute Witness topological features broken down into the time spent to select landmarks, to compute local and global topological features. We find that on all the graphs except Pubmed and OGBN-arXiv, the total computation time is < 9 seconds. On Pubmed, it takes ~ 28 seconds, and on large-scale graph OGBN-arXiv, it takes ~ 96 seconds. These run times are practical given the scale of these graphs (see Table 8, Appendix C).

Datasets/ # Landmarks	Landmark selection time	Local feat. comput. time	Global feat. comput. time
Cora-ML/124	0.01±0.01	0.12±0.03	5.11±0.13
Citeseer/105	0.01±0.01	0.16±0.02	5.23±1.22
Polblogs/61	0.01±0.00	0.07±0.01	4.64±0.2
Snap-patents/91	0.03±0.02	0.64±0.00	7.54±1.15
Pubmed/394	0.07±0.01	0.51±0.03	27.83±0.47
OGBN-arXiv/84	1.02 ±0.00	12.79±0.31	83.04±2.19

Table 6: Efficiency of WGTL. All the times are in seconds.

It is worth noticing that landmark selection is quite efficient, hence not a bottleneck. However, the most expensive part of the computation is the computation of global topological features. We empirically found that this is due to the BFS traversal from $|\mathcal{L}|$ landmarks. One can reduce this cost by selecting fewer landmarks. Another option is to adopt libraries such as RAPIDS cuGraph (Fender, Rees, and Eaton 2022) which uses GPU acceleration for BFS traversal. However, we found negligible improvement in the overall run-time.

5 Conclusion and Future Works

By harnessing the strengths of witness complex to efficiently learn topological representations based on the subset of the most essential nodes as skeleton, we have proposed the novel topological defense against adversarial attacks on graphs, WGTL. WGTL is versatile and can be readily integrated with any GNN architecture or another non-topological defense, leading to substantial gains in robustness. We have derived theoretical properties of WGTL, both at the local and global levels, and have illustrated its utility across a wide range of adversarial attacks.

In future, we plan to explore the utility of WGTL with respect to adversarial learning of time-evolving graphs and hypergraphs. Another interesting research direction is to investigate the linkage between the attacker’s budget, number of landmarks, and topological attacks targeting the skeleton shape, that is, topological properties of the graph induced by the most important nodes (landmarks).

Acknowledgement

This work was supported by the NSF grant TIP-2333703 and the ONR grant N00014-21-1-2530. Also, the paper is based upon work supported by (while Y.R.G. was serving at) the NSF. The views expressed in the article do not necessarily represent the views of NSF or ONR. D. Basu acknowledges the ANR JCJC project REPUBLIC (ANR-22-CE23-0003-01), the PEPR project FOUNDRY (ANR23-PEIA-0003), and the CHIST-ERA project CausalXRL (ANR-21-CHR4-0007).

References

Adams, H.; Emerson, T.; Kirby, M.; Neville, R.; Peterson, C.; Shipman, P.; Chepushtanova, S.; Hanson, E.; Motta, F.; and Ziegelmeier, L. 2017. Persistence images: A stable vector representation of persistent homology. *Journal of Machine Learning Research*, 18.

Arafat, N. A.; Basu, D.; and Bressan, S. 2019. Topological Data Analysis with ϵ -net Induced Lazy Witness Complex. In

International Conference on Database and Expert Systems Applications, 376–392. Springer.

Arafat, N. A.; Basu, D.; and Bressan, S. 2020. ϵ -net Induced Lazy Witness Complexes on Graphs. *arXiv preprint arXiv:2009.13071*.

Bauer, U. 2021. Ripser: efficient computation of Vietoris–Rips persistence barcodes. *Journal of Applied and Computational Topology*, 5(3): 391–423.

Benson, A. R.; Abebe, R.; Schaub, M. T.; Jadbabaie, A.; and Kleinberg, J. 2018. Simplicial closure and higher-order link prediction. *Proceedings of the National Academy of Sciences*, 115(48): E11221–E11230.

Bojchevski, A.; and Günnemann, S. 2019. Adversarial attacks on node embeddings via graph poisoning. In *Proceedings of the International Conference on Machine Learning*, 695–704. PMLR.

Carriere, M.; Chazal, F.; Glisse, M.; Ike, Y.; Kannan, H.; and Umeda, Y. 2021. Optimizing persistent homology based functions. In *Proceedings of the International Conference on Machine Learning*, 1294–1303.

Carrière, M.; Chazal, F.; Ike, Y.; Lacombe, T.; Royer, M.; and Umeda, Y. 2020. Perslay: A neural network layer for persistence diagrams and new graph topological signatures. In *Proceedings of the International Conference on Artificial Intelligence and Statistics*, 2786–2796.

Chazal, F.; Cohen-Steiner, D.; Glisse, M.; Guibas, L. J.; and Oudot, S. Y. 2009. Proximity of persistence modules and their diagrams. In *Proceedings of the twenty-fifth annual symposium on Computational geometry*, 237–246.

Chazal, F.; Cohen-Steiner, D.; Guibas, L. J.; and Oudot, S. 2008. The stability of persistence diagrams revisited.

Chen, D.; O’Bray, L.; and Borgwardt, K. 2022. Structure-aware transformer for graph representation learning. In *Proceedings of the International Conference on Machine Learning*, 3469–3489. PMLR.

Chen, Y.; Coskunuzer, B.; and Gel, Y. 2021. Topological relational learning on graphs. In *Advances in Neural Information Processing systems*, volume 34, 27029–27042.

Chen, Y.; and Gel, Y. R. 2023. Topological Pooling on Graphs. In *AAAI*, volume 37.

Chen, Y.; Sizikova, E.; and Gel, Y. R. 2022. TopoAttn-Nets: Topological Attention in Graph Representation Learning. In *ECML-PKDD*, 309–325.

Chung, Y.-M.; and Lawson, A. 2022. Persistence curves: A canonical framework for summarizing persistence diagrams. *Advances in Computational Mathematics*, 48(1): 6.

Cohen-Steiner, D.; Edelsbrunner, H.; and Harer, J. 2005. Stability of persistence diagrams. In *Proceedings of the Annual Symposium on Computational Geometry*, 263–271.

Cohen-Steiner, D.; Edelsbrunner, H.; Harer, J.; and Mileyko, Y. 2010. Lipschitz functions have L_p -stable persistence. *Foundations of Computational Mathematics*, 10(2): 127–139.

Dai, H.; Li, H.; Tian, T.; Huang, X.; Wang, L.; Zhu, J.; and Song, L. 2018. Adversarial attack on graph structured data. In *Proceedings of the International Conference on Machine Learning*, 1115–1124. PMLR.

- De Silva, V.; and Carlsson, G. 2004. Topological estimation using witness complexes. In *Proceedings of the Eurographics conference on Point-Based Graphics*, 157–166. Eurographics Association.
- Edelsbrunner; Letscher; and Zomorodian. 2002. Topological persistence and simplification. *Discrete & Computational Geometry*, 28: 511–533.
- Engstrom, L.; Ilyas, A.; Santurkar, S.; Tsipras, D.; Tran, B.; and Madry, A. 2019. Adversarial robustness as a prior for learned representations. *arXiv preprint arXiv:1906.00945*.
- Entezari, N.; Al-Sayouri, S. A.; Darvishzadeh, A.; and Papalexakis, E. E. 2020. All you need is low (rank) defending against adversarial attacks on graphs. In *Proceedings of the International Conference on Web Search and Data Mining*, 169–177.
- Fender, A.; Rees, B.; and Eaton, J. 2022. Rapids cugraph. In *Massive Graph Analytics*, 483–493. Chapman and Hall/CRC.
- Feng, B.; Wang, Y.; and Ding, Y. 2021. UAG: Uncertainty-aware attention graph neural network for defending adversarial attacks. *Proceedings of the AAAI Conference on Artificial Intelligence*, 35(8): 7404–7412.
- Feng, F.; He, X.; Tang, J.; and Chua, T.-S. 2019. Graph adversarial training: Dynamically regularizing based on graph structure. *IEEE Transactions on Knowledge and Data Engineering*, 33(6): 2493–2504.
- Gabrielsson, R. B.; Nelson, B. J.; Dwaraknath, A.; and Skraba, P. 2020. A topology layer for machine learning. In *Proceedings of the International Conference on Artificial Intelligence and Statistics*, 1553–1563.
- Gasteiger, J.; Bojchevski, A.; and Günnemann, S. 2018. Predict then propagate: Graph neural networks meet personalized pagerank. *arXiv preprint arXiv:1810.05997*.
- Gebhart, T.; Schrater, P.; and Hylton, A. 2019. Characterizing the shape of activation space in deep neural networks. In *The IEEE International Conference On Machine Learning And Applications*, 1537–1542.
- Geisler, S.; Schmidt, T.; Şirin, H.; Zügner, D.; Bojchevski, A.; and Günnemann, S. 2021. Robustness of graph neural networks at scale. *Advances in Neural Information Processing Systems*, 34: 7637–7649.
- Givens, C. R.; and Shortt, R. M. 1984. A class of Wasserstein metrics for probability distributions. *Michigan Mathematical Journal*, 31(2): 231 – 240.
- Goibert, M.; Ricatte, T.; and Dohmatob, E. 2022. An Adversarial Robustness Perspective on the Topology of Neural Networks. In *ML Safety Workshop at NeurIPS 2022*.
- Günnemann, S. 2022. Graph neural networks: Adversarial robustness. *Graph Neural Networks: Foundations, Frontiers, and Applications*, 149–176.
- Hamilton, W.; Ying, Z.; and Leskovec, J. 2017. Inductive representation learning on large graphs. *Advances in Neural Information Processing Systems*, 30.
- Hausdorff, F. 1914. *Grundzüge der Mengenlehre*, Leipzig.
- Hofer, C.; Graf, F.; Rieck, B.; Niethammer, M.; and Kwitt, R. 2020. Graph filtration learning. In *Proceedings of the International Conference on Machine Learning*, 4314–4323. PMLR.
- Horn, M.; De Brouwer, E.; Moor, M.; Moreau, Y.; Rieck, B.; and Borgwardt, K. 2022. Topological Graph Neural Networks. In *Proceedings of the International Conference on Learning Representations*.
- Hu, W.; Fey, M.; Zitnik, M.; Dong, Y.; Ren, H.; Liu, B.; Catasta, M.; and Leskovec, J. 2020. Open graph benchmark: Datasets for machine learning on graphs. *Advances in Neural Information Processing Systems*, 33: 22118–22133.
- Hu, X.; Li, F.; Samaras, D.; and Chen, C. 2019. Topology-preserving deep image segmentation. In *NeurIPS*, volume 32.
- In, Y.; Yoon, K.; Kim, K.; Shin, K.; and Park, C. 2024. Self-Guided Robust Graph Structure Refinement. In *Proceedings of the ACM on Web Conference 2024*, 697–708.
- Jia, Y.; Zou, D.; Wang, H.; and Jin, H. 2023. Enhancing Node-Level Adversarial Defenses by Lipschitz Regularization of Graph Neural Networks. In *Proceedings of the 28th ACM SIGKDD Conference on Knowledge Discovery and Data Mining*, 951–963.
- Jin, W.; Derr, T.; Wang, Y.; Ma, Y.; Liu, Z.; and Tang, J. 2021a. Node similarity preserving graph convolutional networks. In *Proceedings of the ACM International Conference on Web Search and Data Mining*, 148–156.
- Jin, W.; Li, Y.; Xu, H.; Wang, Y.; Ji, S.; Aggarwal, C.; and Tang, J. 2021b. Adversarial attacks and defenses on graphs. *ACM SIGKDD Explorations Newsletter*, 22(2): 19–34.
- Jin, W.; Ma, Y.; Liu, X.; Tang, X.; Wang, S.; and Tang, J. 2020. Graph structure learning for robust graph neural networks. In *KDD*, 66–74.
- Kipf, T. N.; and Welling, M. 2016. Semi-supervised classification with graph convolutional networks. *arXiv preprint arXiv:1609.02907*.
- Kong, K.; Li, G.; Ding, M.; Wu, Z.; Zhu, C.; Ghanem, B.; Taylor, G.; and Goldstein, T. 2022. Robust Optimization as Data Augmentation for Large-scale Graphs. *arXiv preprint arXiv:2010.09891*.
- Leskovec, J.; Kleinberg, J.; and Faloutsos, C. 2005. Graphs over time: densification laws, shrinking diameters and possible explanations. In *Proceedings of the ACM SIGKDD International Conference on Knowledge Discovery in Data Mining*, 177–187.
- Liu, A.; Li, W.; Li, T.; Li, B.; Huang, H.; and Zhou, P. 2023. Towards Inductive Robustness: Distilling and Fostering Wave-induced Resonance in Transductive GCNs Against Graph Adversarial Attacks. *arXiv preprint arXiv:2312.08651*.
- Liu, S.; Chen, J.; Fu, T.; Lin, L.; Zitnik, M.; and Wu, D. 2024. Graph Adversarial Diffusion Convolution. *arXiv preprint arXiv:2406.02059*.
- Mujkanovic, F.; Geisler, S.; Günnemann, S.; and Bojchevski, A. 2022. Are Defenses for Graph Neural Networks Robust? *Advances in Neural Information Processing Systems*, 35: 8954–8968.
- Rieck, B.; Yates, T.; Bock, C.; Borgwardt, K.; Wolf, G.; Turk-Browne, N.; and Krishnaswamy, S. 2020. Uncovering the

- topology of time-varying fMRI data using cubical persistence. *Advances in Neural Information Processing systems*, 33: 6900–6912.
- Sun, L.; Dou, Y.; Yang, C.; Zhang, K.; Wang, J.; Philip, S. Y.; He, L.; and Li, B. 2022. Adversarial attack and defense on graph data: A survey. *IEEE Transactions on Knowledge and Data Engineering*.
- Tang, X.; Li, Y.; Sun, Y.; Yao, H.; Mitra, P.; and Wang, S. 2020. Transferring robustness for graph neural network against poisoning attacks. In *Proceedings of the International Conference on Web Search and Data Mining*, 600–608.
- Torres, L.; Blevins, A. S.; Bassett, D.; and Eliassi-Rad, T. 2021. The why, how, and when of representations for complex systems. *SIAM Review*, 63(3): 435–485.
- Wang, X.; Cheng, M.; Eaton, J.; Hsieh, C.-J.; and Wu, F. 2018. Attack graph convolutional networks by adding fake nodes. *arXiv preprint arXiv:1810.10751*.
- Wu, F.; Souza, A.; Zhang, T.; Fifty, C.; Yu, T.; and Weinberger, K. 2019a. Simplifying graph convolutional networks. In *Proceedings of the International Conference on Machine Learning*, 6861–6871. PMLR.
- Wu, H.; Wang, C.; Tyshetskiy, Y.; Docherty, A.; Lu, K.; and Zhu, L. 2019b. Adversarial examples for graph data: Deep insights into attack and defense. In *Proceedings of the International Joint Conference on Artificial Intelligence*, 4816–4823.
- Xu, K.; Chen, H.; Liu, S.; Chen, P.-Y.; Weng, T.-W.; Hong, M.; and Lin, X. 2019. Topology Attack and Defense for Graph Neural Networks: An Optimization Perspective. In *Proceedings of the International Joint Conference on Artificial Intelligence*.
- Yan, Z.; Ma, T.; Gao, L.; Tang, Z.; and Chen, C. 2021. Link prediction with persistent homology: An interactive view. In *Proceedings of the International Conference on Machine Learning*, 11659–11669.
- Yan, Z.; Ma, T.; Gao, L.; Tang, Z.; Wang, Y.; and Chen, C. 2022. Neural approximation of extended persistent homology on graphs. In *ICLR 2022 Workshop on Geometrical and Topological Representation Learning*.
- Zhang, A.; and Ma, J. 2020. Defensevae: Defending against adversarial attacks on graph data via a variational graph autoencoder. *arXiv preprint arXiv:2006.08900*.
- Zhang, S.; Xiao, M.; and Wang, H. 2020. GPU-accelerated computation of Vietoris-Rips persistence barcodes. *arXiv preprint arXiv:2003.07989*.
- Zhang, X.; and Zitnik, M. 2020. Gnnguard: Defending graph neural networks against adversarial attacks. *Advances in Neural Information Processing systems*, 33: 9263–9275.
- Zhao, Q.; and Wang, Y. 2019. Learning metrics for persistence-based summaries and applications for graph classification. *Advances in Neural Information Processing Systems*, 32.
- Zhou, Y.; Zheng, H.; Huang, X.; Hao, S.; Li, D.; and Zhao, J. 2022. Graph neural networks: Taxonomy, advances, and trends. *ACM Transactions on Intelligent Systems and Technology*, 13(1): 1–54.
- Zhu, D.; Zhang, Z.; Cui, P.; and Zhu, W. 2019. Robust graph convolutional networks against adversarial attacks. In *Proceedings of the ACM SIGKDD International Conference on Knowledge Discovery & Data Mining*, 1399–1407.
- Zhu, J.; Jin, J.; Loveland, D.; Schaub, M. T.; and Koutra, D. 2022. How does heterophily impact the robustness of graph neural networks? theoretical connections and practical implications. In *Proceedings of the 28th ACM SIGKDD Conference on Knowledge Discovery and Data Mining*, 2637–2647.
- Zhu, J.; Rossi, R. A.; Rao, A.; Mai, T.; Lipka, N.; Ahmed, N. K.; and Koutra, D. 2021. Graph neural networks with heterophily. In *Proceedings of the AAAI conference on Artificial Intelligence*, volume 35, 11168–11176.
- Zhu, J.; Yan, Y.; Zhao, L.; Heimann, M.; Akoglu, L.; and Koutra, D. 2020. Beyond homophily in graph neural networks: Current limitations and effective designs. *Advances in Neural Information Processing Systems*, 33: 7793–7804.
- Zomorodian, A. 2010. Fast construction of the Vietoris-Rips complex. *Computers & Graphics*, 34(3): 263–271.
- Zomorodian, A. J. 2005. *Topology for computing*, volume 16. Cambridge university press.
- Zügner, D.; Akbarnejad, A.; and Günnemann, S. 2018. Adversarial attacks on neural networks for graph data. In *KDD*, 2847–2856.
- Zügner, D.; and Günnemann, S. 2019a. Adversarial Attacks on Graph Neural Networks via Meta Learning. In *Proceedings of the International Conference on Learning Representations*.
- Zügner, D.; and Günnemann, S. 2019b. Certifiable robustness and robust training for graph convolutional networks. In *KDD*, 246–256.

Appendix

A Theoretical Analysis

A.1 Notations

We dedicate Table 7 to index the notations used in this paper. Note that every notation is also defined when it is introduced.

Definition A.1 (Hausdorff distance (Hausdorff 1914)). Let (S, d) be a metric space with metric $d : S \times S \leftarrow \mathbb{R}$. Then, Hausdorff distance between any two non-empty subsets X and Y of S is defined as

$$d_H(X, Y) \triangleq \max \left\{ \sup_{x \in X} \inf_{y \in Y} d(x, y), \sup_{y \in Y} \inf_{x \in X} d(x, y) \right\}.$$

Definition A.2 (p -Wasserstein distance (Givens and Shortt 1984)). Let (S, d) be a Polish space with metric $d : S \times S \leftarrow \mathbb{R}$. Let P and Q be two probability measures on S with finite p -moments for a $p \in [1, \infty)$. Then, p -Wasserstein distance between P and Q is defined as

$$W_p(P, Q) \triangleq \left(\inf_{\gamma \in \Gamma(P, Q)} \int_{S \times S} \|x - y\|^p d\Gamma(x, y) \right)^{1/p},$$

where $\Gamma(P, Q)$ is the set of all couplings of P and Q .

A.2 Properties of the Witness Complexes and Landmarks

We start from presenting the results on the local witness complexes (Arafat, Basu, and Bressan 2020) that are integral for our proofs. Specifically, for a graph \mathcal{G} Theorem A.3 summarises the size of the landmark set, the stability of the landmark set, and the upper bound on the difference of the persistence diagrams obtained through Vietoris-Rips and local witness complexes.

Theorem A.3 (Properties of Local Witness Complexes (Arafat, Basu, and Bressan 2020)). *Let \mathcal{L} be the landmark set computed on a graph \mathcal{G} with $|\mathcal{V}|$ nodes and diameter $\text{Diam}(\mathcal{G})$.*

1. **Finiteness of the landmark set.** *The cardinality of the landmark set \mathcal{L} is $\left(\frac{\text{Diam}(\mathcal{G})}{\epsilon} \right)^{\mathcal{O}(\log \frac{|\mathcal{V}|}{\epsilon})}$. Here, $\epsilon \triangleq \max_{u, v \in \mathcal{L}} \frac{1}{2} d(u, v)$, and is a tunable parameter.*
2. **Stability of the landmark set.** *The Hausdorff distance $d_H(\mathcal{V}, \mathcal{L})$ between connected weighted graph $(\mathcal{V}, d_{\mathcal{G}})$ and its ϵ -net induced subspace $(\mathcal{L}, d_{\mathcal{L}})$ is at most ϵ , where $\mathcal{L} \subseteq \mathcal{V}$ is the set of landmarks.*
3. **3-approximation of Vietoris-Rips.** *For any $\alpha > 2\epsilon \geq 0$, where ϵ corresponds to the ϵ -net induced by the landmark set,*

$$\text{VR}_{\alpha/3}(\mathcal{L}) \subseteq \text{Wit}_{\alpha}(\mathcal{V}, \mathcal{L}) \subseteq \text{VR}_{3\alpha}(\mathcal{L}).$$

That is, $W_{\infty}(\text{PD}_{>2\epsilon}(\text{VR}), \text{PD}_{>2\epsilon}(\text{Wit})) \leq 3 \log 3$, which also implies that

$$W_{\infty}(\text{PD}(\text{VR}(\mathcal{G})), \text{PD}(\text{Wit}(\mathcal{G}))) \leq 3 \log 3 + 2\epsilon. \quad (2)$$

A.3 Stability of the Topological Representations

In this section, we derive stability guarantees of the encoding, computed on a graph \mathcal{G} by the Witness Graph Topological Layer (WGTL) under a perturbation level δ . First, Theorem 3.1 discusses the stability of the local topology encodings (see Figure 2). Then, Theorem 3.2 states the stability of the global topology encodings (see Figure 1). Finally, we leverage these two results to derive the stability of the topological representation learned by WGTL (Figure 1).

Remark A.4. For building Persistence Images, following (Adams et al. 2017), we use Gaussian kernel with variance σ and a weighting function w with $|\nabla w| = 1$. This results in the corresponding $C_{\sigma} \triangleq \left(\sqrt{5} + \sqrt{\frac{10}{\pi} \frac{1}{\sigma}} \right)$, where $\sqrt{5}$ and $\sqrt{10}$ terms arise due to the relations among norms in L^2 and L^{∞} norms. The analysis can be generalized further to other subGaussian kernel, which would lead to modification of the constant C_{σ} .

Theorem 3.1 (Stability of the Local Topology Encoding). *Let us assume that $p < \infty$ and C_{ϵ} is the maximum size of the ϵ -neighbourhood created by the landmarks. Let us denote the persistence diagram obtained from local topology encoding of \mathcal{G} by $T(\mathcal{G})$, and the p -Wasserstein distance between two probability distributions as $W_p(\cdot, \cdot)$.*

(a) If Čech complex, i.e. $\text{Cech}(\mathcal{G})$, is used to compute the local persistence images around each landmark, then for any graph perturbation $\|\mathcal{G} - \mathcal{G}'\|_1 = \mathcal{O}(\delta)$

$$W_p(T(\mathcal{G}), T(\mathcal{G}')) = \mathcal{O}(C_{\epsilon} \delta). \quad (3)$$

(b) If Witness complex, i.e. $\text{Wit}(\mathcal{G})$, is used to compute the local persistence images around each landmark, then for any graph perturbation $\|\mathcal{G} - \mathcal{G}'\|_1 = \mathcal{O}(\delta)$

$$W_p(T(\mathcal{G}), T(\mathcal{G}')) = \mathcal{O}(C_{\epsilon}(\delta + \epsilon)). \quad (4)$$

Proof. By the property of L_p norms, we have

$$W_p(T(\mathcal{G}), T(\mathcal{G}')) \leq W_{\infty}(T(\mathcal{G}), T(\mathcal{G}')), \quad 0 < p < \infty.$$

Let $A(\mathcal{G})$ represent the adjacency matrix constructed from the local topology encoding \mathbf{Z}_{T_L} of the nodes, and $T(\mathcal{G})$ is the persistence diagrams of a fixed dimension $d \in \mathbb{Z}_{\geq 0}$ constructed from $A(\mathcal{G})$. Now, due to the stability theorem of persistence diagrams (Cohen-Steiner, Edelsbrunner, and Harer 2005), we obtain

$$W_{\infty}(T(\mathcal{G}), T(\mathcal{G}')) \leq \|A(\mathcal{G}) - A(\mathcal{G}')\|_{\infty} \leq \|A(\mathcal{G}) - A(\mathcal{G}')\|_1$$

The last inequality holds since $\|\cdot\|_{\infty} \leq \|\cdot\|_1$ for vectors in \mathbb{R}^n .

Thus, we conclude that

$$W_p(T(\mathcal{G}), T(\mathcal{G}')) \leq \|A(\mathcal{G}) - A(\mathcal{G}')\|_1. \quad (5)$$

(a) Čech Complex. Assume that we have access to Čech complexes for each of the ϵ -subgraphs, i.e. \mathcal{G}_l^{ϵ} computed around landmarks $l \in \mathcal{L}$.

Now, we observe that the final adjacency matrix has entries in $\{0, 1\}$. Thus, the transformation from the local persistence

\mathcal{G}	\triangleq A graph with a vertex set \mathcal{V} , an edge set \mathcal{E} , and features \mathbf{X}
N	\triangleq Cardinality of \mathcal{V} , i.e. the number of nodes
F	\triangleq Dimension of features corresponding to each node
\mathbf{A}	\triangleq Adjacency matrix of \mathcal{G}
\mathbf{D}	\triangleq Degree matrix of \mathcal{G}
$d_{\mathcal{G}}(u, v)$	\triangleq Geodesic distance between nodes u and v in graph \mathcal{G}
$\text{Diam}(\mathcal{G})$	\triangleq The diameter of the graph \mathcal{G}
\mathcal{L}	\triangleq The set of landmark nodes
ϵ	\triangleq Radius of the ϵ -net induced on \mathcal{G} by \mathcal{L}
\mathcal{G}_l^ϵ	\triangleq The ϵ -neighborhood of the landmark l in graph \mathcal{G}
C_ϵ	\triangleq Maximum cardinality of the ϵ -neighborhoods induced by the landmarks \mathcal{L}
$d_H(\mathcal{G}_1, \mathcal{G}_2)$	\triangleq Hausdroff distance between graphs \mathcal{G}_1 and \mathcal{G}_2
$W_p(\cdot, \cdot)$	\triangleq p -Wasserstein distance
$\text{PD}(\mathcal{K}(\mathcal{G}))$	\triangleq Persistence diagram of the \mathcal{K} simplicial complexes computed on a graph \mathcal{G} . \mathcal{K} can be Čech, Vietoris-Rips or Witness complex of dimension $d \in \mathbb{Z}_{\geq 0}$.
$\text{PI}(\mathcal{K}(\mathcal{G}))$	\triangleq Persistence image of the \mathcal{K} simplicial complexes computed on a graph \mathcal{G} . In our analysis, \mathcal{K} can be Čech, Vietoris-Rips or Witness complex of $d \in \mathbb{Z}_{\geq 0}$.
$\mathbf{A}(\mathcal{G})$	\triangleq The adjacency matrix constructed from the local topology encoding \mathbf{Z}_{T_L} of the nodes
$\mathbf{T}(\mathcal{G})$	\triangleq Persistence diagrams of dimension $d \in \mathbb{Z}_{\geq 0}$ constructed from $\mathbf{A}(\mathcal{G})$
$\mathbf{A}^{\text{glob}}(\mathcal{G})$	\triangleq The adjacency matrix constructed from the global topology encoding \mathbf{Z}_{T_G} of the nodes
C_σ	\triangleq constant introduced due to kernelization of the persistent images, e.g., for Gaussian kernels $C_\sigma = \left(\sqrt{5} + \sqrt{\frac{10}{\pi} \frac{1}{\sigma}}\right)$.

Table 7: Notations.

images to the final adjacency matrices computed using Local Topology Encodings is 1-Lipschitz. Hence,

$$\begin{aligned} \|A(\mathcal{G}) - A(\mathcal{G}')\|_1 &\leq \sum_{i=1}^{|\mathcal{V}|} \|\text{PI}(\text{Cech}(\mathcal{G}_i) - \text{PI}(\text{Cech}(\mathcal{G}'_i))\|_1 \\ &= \sum_{l=1}^{|\mathcal{L}|} |\mathcal{G}_l^\epsilon| \|\text{PI}(\text{Cech}(\mathcal{G}_l^\epsilon) - \text{PI}(\text{Cech}(\mathcal{G}'_l^\epsilon))\|_1. \end{aligned}$$

The final equality is due to the fact that by construction of the local topology encodings, the persistence images for all nodes $i \in \mathcal{G}_l^\epsilon$ are the same.

Now, as a direct consequence of the stability theorem of the persistence images (Adams et al. 2017, Theorem 10), we obtain

$$\begin{aligned} &\sum_{l=1}^{|\mathcal{L}|} |\mathcal{G}_l^\epsilon| \times \|\text{PI}(\text{Cech}(\mathcal{G}_l^\epsilon) - \text{PI}(\text{Cech}(\mathcal{G}'_l^\epsilon))\|_1 \\ &\leq C_\sigma \sum_{l=1}^{|\mathcal{L}|} |\mathcal{G}_l^\epsilon| \times W_1(\text{PD}(\text{Cech}(\mathcal{G}_l^\epsilon), \text{PD}(\text{Cech}(\mathcal{G}'_l^\epsilon))) \\ &\leq C_\sigma \sum_{l=1}^{|\mathcal{L}|} |\mathcal{G}_l^\epsilon| \times W_\infty(\text{PD}(\text{Cech}(\mathcal{G}_l^\epsilon), \text{PD}(\text{Cech}(\mathcal{G}'_l^\epsilon))). \end{aligned}$$

Finally, by applying the stability theorem of persistence diagrams (Cohen-Steiner, Edelsbrunner, and Harer 2005) on each of the ϵ -neighborhoods of the landmarks, we find

$$\begin{aligned} &\sum_{l=1}^{|\mathcal{L}|} |\mathcal{G}_l^\epsilon| \times W_\infty(\text{PD}(\text{Cech}(\mathcal{G}_l^\epsilon), \text{PD}(\text{Cech}(\mathcal{G}'_l^\epsilon))) \\ &\leq \sum_{l=1}^{|\mathcal{L}|} |\mathcal{G}_l^\epsilon| \times \|\mathcal{G}_l^\epsilon - \mathcal{G}'_l^\epsilon\|_\infty \end{aligned}$$

$$\begin{aligned} &\leq \sum_{l=1}^{|\mathcal{L}|} |\mathcal{G}_l^\epsilon| \times \|\mathcal{G}_l^\epsilon - \mathcal{G}'_l^\epsilon\|_1 \\ &\leq \max_l |\mathcal{G}_l^\epsilon| \|\mathcal{G} - \mathcal{G}'\|_1 = \mathcal{O}(C_\epsilon \|\mathcal{G} - \mathcal{G}'\|_1). \end{aligned}$$

The last two inequalities hold due to the fact that $\|x\|_\infty \leq \|x\|_1$ and $\sum_{i=1}^m a_i b_i \leq \left(\max_{i \in \{1, \dots, m\}} a_i\right) \sum_{i=1}^m b_i$ if $0 \leq a_i, b_i < \infty$, respectively.

Thus, using Equation (5), we conclude that

$$W_p(\mathbf{T}(\mathcal{G}), \mathbf{T}(\mathcal{G}')) = \mathcal{O}(C_\epsilon \|\mathcal{G} - \mathcal{G}'\|_1).$$

(b) *Witness Complex.* Now, we consider the scenario where we have access to only the local Witness complexes as it happens in WGT. Specifically, we assume that we have access to Witness complexes $\text{Wit}(\mathcal{G}_l^\epsilon)$ for each of the ϵ -subgraphs, i.e. \mathcal{G}_l^ϵ computed around landmarks $l \in \mathcal{L}$. Then, due to the 1-Lipschitzness of the mapping from the persistence images of the Witness complex to the adjacency matrix, we get

$$\|A(\mathcal{G}) - A(\mathcal{G}')\|_1 \leq \sum_{l=1}^{|\mathcal{L}|} |\mathcal{G}_l^\epsilon| \times \|\text{PI}(\text{Wit}(\mathcal{G}_l^\epsilon)) - \text{PI}(\text{Wit}(\mathcal{G}'_l^\epsilon))\|_1.$$

Now, similarly applying the relation between the persistence images and persistence diagrams (Adams et al. 2017, Theorem 10), we obtain

$$\begin{aligned} &\sum_{l=1}^{|\mathcal{L}|} |\mathcal{G}_l^\epsilon| \times \|\text{PI}(\text{Wit}(\mathcal{G}_l^\epsilon)) - \text{PI}(\text{Wit}(\mathcal{G}'_l^\epsilon))\|_1 \quad (6) \\ &\leq C_\sigma \sum_{l=1}^{|\mathcal{L}|} |\mathcal{G}_l^\epsilon| \times W_1(\text{PD}(\text{Wit}(\mathcal{G}_l^\epsilon)), \text{PD}(\text{Wit}(\mathcal{G}'_l^\epsilon))) \\ &\leq C_\sigma \sum_{l=1}^{|\mathcal{L}|} |\mathcal{G}_l^\epsilon| \times W_\infty(\text{PD}(\text{Wit}(\mathcal{G}_l^\epsilon)), \text{PD}(\text{Wit}(\mathcal{G}'_l^\epsilon))). \quad (7) \end{aligned}$$

Now, using the relation between the Vietoris-Rips and the Witness complexes (as in Theorem A.3.3.) as well as the triangle inequality, we observe that

$$\begin{aligned} & W_\infty(\text{PD}(\text{Wit}(\mathcal{G}_i^\epsilon)), \text{PD}(\text{Wit}(\mathcal{G}'_i^\epsilon))) \\ & \leq 2W_\infty(\text{PD}(\text{VR}(\mathcal{G}_i^\epsilon)), \text{PD}(\text{VR}(\mathcal{G}'_i^\epsilon))) + 6\log 3 + 4\epsilon. \end{aligned}$$

Further application of the stability theorem of persistence diagrams constructed from Vietoris-Rips complex (Chazal et al. 2009) yields

$$\begin{aligned} & W_\infty(\text{PD}(\text{Wit}(\mathcal{G}_i^\epsilon)), \text{PD}(\text{Wit}(\mathcal{G}'_i^\epsilon))) \\ & \leq 2\|\mathcal{G}_i^\epsilon - \mathcal{G}'_i^\epsilon\|_\infty + 6\log 3 + 4\epsilon \\ & \leq 2\|\mathcal{G}_i^\epsilon - \mathcal{G}'_i^\epsilon\|_1 + 6\log 3 + 4\epsilon, \end{aligned} \quad (8)$$

where ϵ corresponds to the ϵ -net induced by the landmark set \mathcal{L} on the graphs \mathcal{G} .

Combining Equations (7) and (8) results in

$$\begin{aligned} & \|A(\mathcal{G}) - A(\mathcal{G}')\|_1 \\ & \leq \sum_{l=1}^{|\mathcal{L}|} |\mathcal{G}_l^\epsilon| \times \|\text{PI}(\text{Wit}(\mathcal{G}_l^\epsilon)) - \text{PI}(\text{Wit}(\mathcal{G}'_l^\epsilon))\|_1 \\ & \leq C_\sigma \sum_{l=1}^{|\mathcal{L}|} |\mathcal{G}_l^\epsilon| \times (2\|\mathcal{G}_l^\epsilon - \mathcal{G}'_l^\epsilon\|_1 + 6\log 3 + 4\epsilon) \\ & \leq C_\sigma \max_l |\mathcal{G}_l^\epsilon| (2\|\mathcal{G} - \mathcal{G}'\|_1 + 6\log 3 + 4\epsilon) \\ & \leq C_\sigma C_\epsilon \max_l |\mathcal{G}_l^\epsilon| (2\|\mathcal{G} - \mathcal{G}'\|_1 + 6\log 3 + 4\epsilon). \end{aligned} \quad (9)$$

Armed the result in Equation (5), we conclude that

$$W_p(\text{T}(\mathcal{G}), \text{T}(\mathcal{G}')) = \mathcal{O}(C_\epsilon (\|\mathcal{G} - \mathcal{G}'\|_1 + \epsilon)).$$

□

Proposition 3.2 (Stability of the Global Topology Encoding). *(a) If we have access to the Čech simplicial complex $\text{Cech}^{\text{glob}}(\mathcal{G})$ for \mathcal{G} , then for any graph perturbation $\|\mathcal{G} - \mathcal{G}'\|_1 = \mathcal{O}(\delta)$ the global topology encoding satisfies*

$$\|\text{PI}(\text{Cech}^{\text{glob}}(\mathcal{G})) - \text{PI}(\text{Cech}^{\text{glob}}(\mathcal{G}'))\|_\infty = \mathcal{O}(\delta).$$

(b) If the landmarks \mathcal{L} selected to compute the global Witness complex $\text{Wit}^{\text{glob}}(\mathcal{G})$ induce an ϵ -net of the graph \mathcal{G} with $\epsilon > 0$, then for any graph perturbation $\|\mathcal{G} - \mathcal{G}'\|_1 = \mathcal{O}(\delta)$ the global topology encoding satisfies

$$\|\text{PI}(\text{Wit}^{\text{glob}}(\mathcal{G})) - \text{PI}(\text{Wit}^{\text{glob}}(\mathcal{G}'))\|_\infty = \mathcal{O}(\delta + \epsilon). \quad (10)$$

Proof.

Part (a). Let us first prove the results for the condition where we have access to the Čech complex $\text{Cech}^{\text{glob}}(\mathcal{G})$ on graph \mathcal{G} . We denote the global persistence image computed from the witness complex on $\text{Cech}^{\text{glob}}(\mathcal{G})$.

Then,

$$\begin{aligned} & \|\text{PI}(\text{Cech}^{\text{glob}}(\mathcal{G})) - \text{PI}(\text{Cech}^{\text{glob}}(\mathcal{G}'))\|_\infty \\ & \leq \|\text{PI}(\text{Cech}^{\text{glob}}(\mathcal{G})) - \text{PI}(\text{Cech}^{\text{glob}}(\mathcal{G}'))\|_1 \\ & \leq C_\sigma W_1 \left(\text{PD}(\text{Cech}^{\text{glob}}(\mathcal{G})), \text{PD}(\text{Cech}^{\text{glob}}(\mathcal{G}')) \right). \end{aligned}$$

Here the first inequality is due to the fact that $\|\cdot\|_\infty \leq \|\cdot\|_1$ for vectors in \mathbb{R}^n . The second inequality is due to the stability

theorem of persistence images with Gaussian kernels (Adams et al. 2017, Theorem 10).

Now, applying the relation between W_∞ and W_1 distances, we get

$$\begin{aligned} & W_1 \left(\text{PD}(\text{Cech}^{\text{glob}}(\mathcal{G})), \text{PD}(\text{Cech}^{\text{glob}}(\mathcal{G}')) \right) \\ & \leq W_\infty \left(\text{PD}(\text{Cech}^{\text{glob}}(\mathcal{G})), \text{PD}(\text{Cech}^{\text{glob}}(\mathcal{G}')) \right). \end{aligned}$$

Now, by applying the stability theorem of persistence diagram of Vietoris-Rips complex (Chazal et al. 2009), we arrive to

$$\begin{aligned} & W_\infty \left(\text{PD}(\text{Cech}^{\text{glob}}(\mathcal{G})), \text{PD}(\text{Cech}^{\text{glob}}(\mathcal{G}')) \right) \\ & \leq \|\mathcal{G} - \mathcal{G}'\|_\infty \leq \|\mathcal{G} - \mathcal{G}'\|_1 = \mathcal{O}(\delta). \end{aligned}$$

Part b: Witness complex. Following the similar steps as the derivation for Čech complex, we get

$$\begin{aligned} & \|\text{PI}(\text{Wit}^{\text{glob}}(\mathcal{G})) - \text{PI}(\text{Wit}^{\text{glob}}(\mathcal{G}'))\|_\infty \\ & \leq W_\infty \left(\text{PD}(\text{Wit}^{\text{glob}}(\mathcal{G})), \text{PD}(\text{Wit}^{\text{glob}}(\mathcal{G}')) \right). \end{aligned}$$

Due to the 3-approximation theorem of Vietoris-Rips complex with Witness complex (Theorem A.3.3.), we find

$$\begin{aligned} & W_\infty \left(\text{PD}(\text{Wit}^{\text{glob}}(\mathcal{G})), \text{PD}(\text{Wit}^{\text{glob}}(\mathcal{G}')) \right) \\ & \leq 2W_\infty \left(\text{PD}(\text{VR}^{\text{glob}}(\mathcal{G})), \text{PD}(\text{VR}^{\text{glob}}(\mathcal{G}')) \right) + 6\log 3 + 4\epsilon. \end{aligned}$$

Now, by applying the stability theorem of persistence diagram of Vietoris-Rips complex (Chazal et al. 2009), we get

$$\begin{aligned} & W_\infty \left(\text{PD}(\text{VR}^{\text{glob}}(\mathcal{G})), \text{PD}(\text{VR}^{\text{glob}}(\mathcal{G}')) \right) \\ & \leq \|\mathcal{G} - \mathcal{G}'\|_\infty \leq \|\mathcal{G} - \mathcal{G}'\|_1 = \mathcal{O}(\delta). \end{aligned}$$

Combining these steps, we conclude that

$$\|\text{PI}(\text{Wit}^{\text{glob}}(\mathcal{G})) - \text{PI}(\text{Wit}^{\text{glob}}(\mathcal{G}'))\|_\infty = \mathcal{O}(\delta + \epsilon).$$

□

Proposition 3.3 (Stability of the attention-driven node representation in Figure 1). *If the landmarks selected for the Witness complex induce an ϵ -net of the graph with $\epsilon > 0$, we obtain that for any graph perturbation $\|\mathcal{G} - \mathcal{G}'\|_1 = \mathcal{O}(\delta)$ the global topology encoding satisfies*

$$\|\mathbf{Z}_{\text{WGT}}(\mathcal{G}) - \mathbf{Z}_{\text{WGT}}(\mathcal{G}')\|_1 = \mathcal{O}(C_\epsilon (C_\epsilon + L_{\text{GNN}})(\delta + \epsilon)^2). \quad (11)$$

Proof. We proceed with the proof in three steps.

Step 1: Decomposition to three components. We begin the proof by decomposing the WGT representation of \mathcal{G} into its three components. Specifically,

$$\mathbf{Z}_{\text{WGT}}(\mathcal{G}) = (\alpha_{T_L} \mathbf{A}(\mathcal{G}) + \alpha_G \mathbf{A}^{\text{GNN}}(\mathcal{G})) \mathbf{A}^{\text{glob}}(\mathcal{G}),$$

where $\mathbf{A}(\mathcal{G})$ represents the adjacency matrix constructed from the local topology encoding \mathbf{Z}_{T_L} of the nodes, $\mathbf{A}^{\text{glob}}(\mathcal{G})$ represents the adjacency matrix constructed from the global topology encoding \mathbf{Z}_{T_G} of the nodes, \mathbf{A}^{GNN} represents the adjacency matrix constructed from the encoding $\mathbf{Z}_G^{(m+1)}$

of the nodes obtained from GNNs, and α_{T_L} and α_G are non-negative attention weights in $(0, 1)$ as described in Section 3.1.

Step 2: Stability of the three individual components. In order to prove the stability of the WGTl representation, we first prove the stability results of each of the components.

1. For the local PIs passing through transformer, we have from Equation (9)

$$\|\mathbf{A}(\mathcal{G}) - \mathbf{A}(\mathcal{G}')\|_1 \leq C_\sigma C_\epsilon (\|\mathcal{G} - \mathcal{G}'\|_1 + 6 \log 3 + 4\epsilon).$$

The constants follow directly from Theorem 3.1.

2. For the global PIs passing through CNN, we have from Proposition 3.2

$$\|\mathbf{A}^{glob}(\mathcal{G}) - \mathbf{A}^{glob}(\mathcal{G}')\|_\infty \leq C_\sigma (\|\mathcal{G} - \mathcal{G}'\|_1 + 6 \log 3 + 4\epsilon).$$

The constants follow the Proposition 3.2.

3. For the graph passing through GNN, following (Jia et al. 2023), we obtain

$$\|\mathbf{A}^{GNN}(\mathcal{G}) - \mathbf{A}^{GNN}(\mathcal{G}')\|_1 \leq L_{GNN} \|\mathcal{G} - \mathcal{G}'\|_1.$$

Step 3: Merging the pieces together.

$$\begin{aligned} & \|\mathbf{Z}_{WGTl}(\mathcal{G}) - \mathbf{Z}_{WGTl}(\mathcal{G}')\|_1 \\ &= \|(\alpha_{T_L} \mathbf{A}(\mathcal{G}) + \alpha_G \mathbf{A}^{GNN}) \mathbf{A}^{glob}(\mathcal{G}) \\ & \quad - (\alpha_{T_L} \mathbf{A}(\mathcal{G}') + \alpha_G \mathbf{A}^{GNN}(\mathcal{G}')) \mathbf{A}^{glob}(\mathcal{G}')\|_1 \\ &\stackrel{(a)}{\leq} \|(\alpha_{T_L} \mathbf{A}(\mathcal{G}) + \alpha_G \mathbf{A}^{GNN}) - (\alpha_{T_L} \mathbf{A}(\mathcal{G}') + \alpha_G \mathbf{A}^{GNN}(\mathcal{G}'))\|_1 \\ & \quad \times \|\mathbf{A}^{glob}(\mathcal{G}) - \mathbf{A}^{glob}(\mathcal{G}')\|_\infty \\ &\stackrel{(b)}{\leq} (\|\mathbf{A}(\mathcal{G}) - \mathbf{A}(\mathcal{G}')\|_1 + \|\mathbf{A}^{GNN} - \mathbf{A}^{GNN}(\mathcal{G}')\|_1) \\ & \quad \times \|\mathbf{A}^{glob}(\mathcal{G}) - \mathbf{A}^{glob}(\mathcal{G}')\|_\infty \\ &= \mathcal{O}((C_\epsilon(\delta + \epsilon) + L_{GNN}\delta) C_\epsilon(\delta + \epsilon)) \\ &= \mathcal{O}((C_\epsilon + L_{GNN}) C_\epsilon(\delta + \epsilon)^2) \end{aligned}$$

Inequality (a) is due to Hölder's inequality. Inequality (b) is due to triangle inequality.

The final result is due to a direct application of the results in Step 2. \square

A.4 Stability of the Topological Loss

In this section, we derive the stability bounds on the topological loss (Equation (1)) incurred due to perturbation of the underlying graph \mathcal{G} by an amount δ . In order to derive the stability result (Proposition 3.4), we first bound the topological loss incurred due to a graph \mathcal{G} and its dependence on the properties of the graph \mathcal{G} (Theorem A.5).

Theorem A.5 (Boundedness of Topological Loss). *Let us assume that the cardinality of the ϵ -neighborhood of any node in \mathcal{G} grows polynomially, i.e. $C_\epsilon = \mathcal{O}(\epsilon^{-M})$ for an $M > 0$. If m is the number of points in the persistence diagram, $k = \max\{p, q\}$ and $2k > M$, $L_{topo,k}(\mathbf{T}(\mathcal{G}))$ is bounded, such that*

$$L_{topo,k}(\mathbf{T}(\mathcal{G})) \leq C_\sigma^{2k} \epsilon^{-2kM} \text{Diam}(A(\mathcal{G})) + 2^{k-2} m \text{Diam}(\mathcal{G})^{2k}. \quad (12)$$

Proof. We proceed with the proof in three steps.

Step 1: Decomposition. First, we decompose the impacts of persistence and birth of complexes on the topological loss by applying a series of algebraic inequalities.

$$\begin{aligned} & L_{topo,k}(\mathbf{T}(\mathcal{G})) \quad (13) \\ &= \sum_{i=1}^m (d_i - b_i)^p \left(\frac{d_i + b_i}{2} \right)^q \\ &\stackrel{(a)}{\leq} \sum_{i=1}^m \frac{(d_i - b_i)^{2p}}{2} + \frac{1}{2} \left(\frac{d_i + b_i}{2} \right)^{2q} \\ &\stackrel{(b)}{\leq} \sum_{i=1}^m \frac{(d_i - b_i)^{2p}}{2} + 2^{q-1} \left(b_i^{2q} + \left(\frac{d_i - b_i}{2} \right)^{2q} \right) \\ &\leq \sum_{i=1}^m \left(1 + \frac{1}{2^q} \right) \frac{(d_i - b_i)^{\max\{2p, 2q\}}}{2} + 2^{q-1} \sum_{i=1}^m b_i^{2q} \\ &= \frac{1}{2} \left(1 + \frac{1}{2^q} \right) \sum_{i=1}^m (d_i - b_i)^{\max\{2p, 2q\}} + 2^{q-1} \sum_{i=1}^m b_i^{2q} \\ &\stackrel{(c)}{\leq} \sum_{i=1}^m (d_i - b_i)^{2k} + 2^{q-1} \sum_{i=1}^m b_i^{2q}. \quad (14) \end{aligned}$$

Step (a) is due to the fact that $2xy \leq x^2 + y^2$ for all $x, y \in \mathbb{R}$.

Step (b) holds true as $\left(\frac{x+y}{2} \right)^{2q} = \left(\frac{x-y}{2} + y \right)^{2q} \leq 2^{q-1} \left(\left(\frac{x-y}{2} \right)^{2q} + y^{2q} \right)$ for $x, y \geq 0$ and $q \geq 1$.

The last inequality (c) holds due to the fact that for any $q \geq 0$, $\frac{1}{2} \left(1 + \frac{1}{2^q} \right) \leq 1$.

Step 2: Controlling impacts of persistence and births.

Due to (Cohen-Steiner et al. 2010), we know that degree $2k$ -total persistence for any Lipschitz function f over a triangulable compact metric space Dom is upper bounded by $C_{Dom} \text{Lip}(f)^{2k}$ for $2k > M$ is bounded by

$$\sum_{i=1}^m (d_i - b_i)^{2k} \leq C_{A(\mathcal{G})} \text{Lip}(A(\mathcal{G}))^{2k} \leq C_\sigma^{2k} C_\epsilon^{2k} \text{Diam}(A(\mathcal{G})). \quad (15)$$

The second inequality is due to the Lipschitzness property of persistence images (Adams et al. 2017, Theorem 4) applied on the local persistence images calculated on an ϵ -neighborhood. Thus, $\text{Lip}(A(\mathcal{G})) \leq C_\sigma C_\epsilon$, where C_ϵ is the maximum cardinality of the ϵ -neighborhoods induced by the landmarks.

We also know that the birth and death of topological features on a graph \mathcal{G} is upper bounded by the diameter of the graph $\text{Diam}(\mathcal{G})$, as mentioned in Section 2. Thus,

$$\sum_{i=1}^m b_i^{2q} \leq m \text{Diam}(\mathcal{G})^{2q} \leq m \text{Diam}(\mathcal{G})^{2k}. \quad (16)$$

Step 3: Merging it together. Finally, by applying Equation (15) and (16) in Equation (14), we get

$$\begin{aligned} & L_{topo,k}(\mathbf{T}(\mathcal{G})) = \\ & \mathcal{O} \left(C_\sigma^{2k} \epsilon^{-2kM} \text{Diam}(A(\mathcal{G})) + 2^{k-1} m \text{Diam}(\mathcal{G})^{2k} \right). \end{aligned}$$

\square

Proposition 3.4 (Stability of Topological Loss). *Let us assume that the cardinality of the ϵ -neighborhood of any node in \mathcal{G} grows polynomially, i.e. $C_\epsilon = \mathcal{O}(\epsilon^{-M})$ for an $M > 0$. If m is the number of points in the persistence diagram, $k = \max\{p, q\}$ and $2k > M$, $L_{topo,k}(\mathcal{T}(\mathcal{G}))$ is bounded, such that*

$$|L_{topo,k}(\mathcal{T}(\mathcal{G})) - L_{topo,k}(\mathcal{T}(\mathcal{G}'))| = \mathcal{O}\left(C_\epsilon \left(C_\sigma^{2k} \epsilon^{-2kM} \text{Diam}(\mathcal{A}(\mathcal{G})) + 2^{k-1} m \text{Diam}(\mathcal{G})^{2k}\right) \|\mathcal{G} - \mathcal{G}'\|_1\right)$$

Proof. By Theorem A.5, we know that $L_{topo,k}(\mathcal{T}(\mathcal{G}))$ is a bounded function, where the upper bound depends on diameter of the graph \mathcal{G} and the corresponding local topology encoding $\mathcal{A}(\mathcal{G})$. For simplicity, let us denote the bound by $B(\mathcal{G})$.

Since every bounded function is Lipschitz with the worst possible Lipschitz constant being the bound itself, we get

$$\begin{aligned} & |L_{topo,k}(\mathcal{T}(\mathcal{G})) - L_{topo,k}(\mathcal{T}(\mathcal{G}'))| \\ & \leq B(\mathcal{G}) \|\mathcal{A}(\mathcal{G}) - \mathcal{A}(\mathcal{G}')\|_\infty = \mathcal{O}(B(\mathcal{G}) C_\epsilon \|\mathcal{G} - \mathcal{G}'\|_1). \end{aligned}$$

The last statement holds true due to Equation 9. We conclude the proof by replacing $B(\mathcal{G})$ with the exact expression in Equation 12. \square

B Details of Adversarial Attacks: Configurations and Budgets

There are many adversarial attacks in the literature (Zhou et al. 2022; Jin et al. 2021b; Zügner and Günnemann 2019a; Mujkanovic et al. 2022; Zügner, Akbarnejad, and Günnemann 2018; Wu et al. 2019b). In this paper, we validate our method for poisoning-type attacks. Other types of attacks, such as node-injection (Wang et al. 2018), reinforcement-learning-based attacks (Dai et al. 2018) and attacks on node-embeddings (Bojchevski and Günnemann 2019) are left as future work.

In this paper, we focus on four different local and global poisoning attacks to evaluate the robustness of our proposed WGTL, and consider a fixed GCN without weight re-training as the surrogate for all attacks. All attacks are considered under a non-adaptive setting, meaning it is assumed that the attacker can not adapt or interact with the model during the attack process. In all the poisoning attacks, we vary the perturbation rate, i.e., the ratio of changed edges, from 0% to 10% with a step of 5%.

Global Poisoning Attacks. Among global (non-targeted) poisoning attacks, we consider metattack (Zügner and Günnemann 2019a) and two different topological attacks: PGD (Xu et al. 2019) and its more recent adaptation Meta-PGD (Mujkanovic et al. 2022). Metattack treats the graph as a hyperparameter and greedily selects perturbations based on meta-gradient for node pairs until the budget is exhausted. PGD attack (Xu et al. 2019) uses the Projected Gradient Descent algorithm with the constraint $\|\mathbf{S}\|_0 \leq \delta$ to minimise attacker loss. Here, \mathbf{S} is a binary symmetric matrix with $S_{ij} = 1$ if the (i, j) -th entry of the Adjacency matrix is flipped by the attacker, and 0 otherwise. Recently, (Mujkanovic et al. 2022) proposes to apply PGD on the meta-gradients to design attacks stronger than the greedy metattack.

Meta-PGD has been shown to be more effective than metattack in many cases (Mujkanovic et al. 2022). Hence, we consider it a more challenging poisoning attack for the proposed method.

To perform metattack, we keep all the default parameter settings (e.g., $\lambda = 0$) following the original implementation (Zügner and Günnemann 2019a). For Cora-ML, Citeseer and Polblogs, we apply the Meta-Self variant of metattack since it is the most effective metattack variant, while for Pubmed, the approximate version of Meta-Self, A-Meta-Self, is applied to save memory and time (Jin et al. 2020). We perform the PGD attack with the CE-type attacker loss function. Following the implementation (Xu et al. 2019), we keep their default parameter settings, i.e., the number of iterations $T = 200$ and learning rate $\eta_t = 200/\sqrt{t}$. For Meta-PGD, we keep the same parameter settings as (Mujkanovic et al. 2022), i.e., a learning rate of 0.01 and gradient clipping threshold of 1.

Local Poisoning Attack. Among local attacks, we use netattack (Zügner, Akbarnejad, and Günnemann 2018). Netattack is a targeted attack which first selects possible perturbation candidates not violating degree distribution and feature co-occurrence of the original graph. Then, it greedily selects, until the attacker’s budget is exhausted, the perturbation with the largest score to modify the graph. The score function is the difference in the log probabilities of a target node.

Following Zügner, Akbarnejad, and Günnemann (2018), we vary the number of perturbations made on every targeted node from 1 to 2 with a step size of 1. Following (Jin et al. 2020), the nodes in the test set with a degree > 10 are treated as target nodes. We only sample 10% of them to reduce the running time of netattack on Pubmed, while for other datasets, we use all the target nodes.

C Experimental Details

Experimental Setup. All experiments are run on a server with 32 Intel(R) Xeon(R) Silver 4110 CPU @ 2.10GHz processors, 256 GB RAM, and an NVIDIA GPU card with 24GB GPU memory. All models are trained on a single GPU.

Datasets. Following Zügner, Akbarnejad, and Günnemann (2018); Zügner and Günnemann (2019a); Jin et al. (2020), we validate the proposed approach on 6 benchmark datasets: 5 homophilic and 1 heterophilic graph. The homophilic graph includes three citation graphs: Citeseer, Cora, and Pubmed, one blog graph: Polblogs, and one large-scale graph from Open-Graph Benchmark (OGB): OGBN-arXiv (Hu et al. 2020). As heterophilic graph dataset, we consider Snap-patents (Leskovec, Kleinberg, and Faloutsos 2005). For each graph, we randomly choose 10% of nodes for training, 10% of nodes for validation, and the remaining 80% of nodes for testing. For each experiment, we report the average accuracy of 10 runs. Note that in the Polblogs graph node features are not available. Following Jin et al. (2020), we set the attribute matrix to $N \times N$ identity matrix.

D Ablation studies

To evaluate the contributions of the different components in our WTGL, we perform ablation studies on Cora-ML and Polblogs datasets under a global attack, i.e., metattack, and a

Dataset	#nodes (LCC)	#edges (LCC)	#classes	#features
Cora-ML	2,485	5,069	7	1,433
Citeseer	2,110	3,668	6	3,703
Pubmed	19,717	44,338	3	500
Polblogs	1,222	16,714	2	None
OGBN-arXiv	169,343	1,157,799	40	128
Snap-patents	4562	12103	5	269

Table 8: Dataset statistics: only the largest connected component (LCC) is considered.

local attack, i.e., netattack. We use GCN as the backbone architecture and consider three ablated variants: (i) GCN+Local Topology Encoding (LTE), (ii) GCN+Global Topology Encoding (GTE), and (iii) GCN+LTE+GTE+Topological Loss (TopoLoss) (i.e., GCN + WTGL).

The experimental results for metattack and netattack are shown in Table 9 and Table 10 respectively. Consistent improvement from the backbone GCN while using GTE, LTE, and topological loss together suggest their importance in an individual as well as in an aggregated manner.

Dataset	Model	Perturbation rate		
		0%	5%	10%
Cora-ML	GCN	82.87±0.83	76.55±0.79	70.39±1.28
	GCN + LTE	83.26±0.43	77.35±0.38	71.27±0.81
	GCN + GTE	83.37±1.12	77.78±0.59	70.66±1.76
	GCN + LTE + GTE + TopoLoss	83.83±0.55	78.63±0.76	73.41±0.82
Polblogs	GCN	94.40±1.47	71.41±2.42	69.16±1.86
	GCN + LTE	95.34±0.73	72.27±1.07	72.02±0.97
	GCN + GTE	95.07±0.09	72.78±0.57	73.14±1.59
	GCN + LTE + GTE + TopoLoss	95.95±0.15	72.84±0.86	74.62±0.42

Table 9: Ablation studies (Accuracy±Std) on datasets under Metattack.

Datasets	Model	Number of perturbations per node		
		0	1	2
Cora-ML	GCN	82.87±0.93	82.53±1.06	82.08±0.81
	GCN + LTE	82.88±0.24	82.56±0.13	82.33±0.33
	GCN + GTE	83.15±0.43	82.42±0.66	82.29±0.48
	GCN + LTE + GTE + TopoLoss	83.83±0.55	83.41±0.87	82.74±0.65
Polblogs	GCN	94.40±1.48	88.91±1.06	85.39±0.86
	GCN + LTE	95.42±0.58	91.45±0.56	88.40±0.94
	GCN + GTE	95.07±0.11	91.47±0.68	89.10±0.70
	GCN + LTE + GTE + TopoLoss	95.95±0.15	91.47±0.33	89.10±0.69

Table 10: Performance (Accuracy±Std) on Cora-ML under Netattack.

E Impact of landmark selection algorithm

The pseudocode for selecting landmarks for computing global witness topological features and local witness topological features is presented in Algorithm 1. In order to compute global witness features, we select a set of *global landmark* nodes. In order to compute local witness features, we select a set of *local landmark* nodes for each node in the graph.

In Lines 1-3, we select the set of global landmarks \mathcal{L}_g in order to construct Global witness filtration. We select the topmost $p\%$ highest degree nodes in the graph \mathcal{G} as landmarks.

Algorithm 1: Greedy Landmark selection algorithm

Input: Graph $\mathcal{G} = (\mathcal{V}, \mathcal{E})$, % of nodes as landmarks $p \in (0, 1)$
Output: Global landmark set \mathcal{L}_g and Local landmark set \mathcal{L}

- 1: Number of landmarks $n_g \leftarrow |\mathcal{V}| \cdot p$
- 2: Sort \mathcal{V} in decreasing order of node degrees.
- 3: Select Global Landmarks $\mathcal{L}_g \leftarrow \mathcal{V}[1, 2, \dots, n_g]$
- 4: **for all** $l \in \mathcal{L}_g$ **do**
- 5: Compute cover $C_l \leftarrow \{u \in \mathcal{V} : d_{\mathcal{G}}(u, l) < d_{\mathcal{G}}(u, l') \ \forall l' \in \mathcal{L}_g \setminus \{l\}\}$
- 6: Compute Subgraph $G_l \leftarrow \mathcal{G}[C_l]$
- 7: Number of local landmarks $n_l \leftarrow |C_l| \cdot p$
- 8: Sort C_l in decreasing order of node degrees in G_l .
- 9: Select Local landmarks $\mathcal{L}[l] \leftarrow C_l[1, \dots, n_l]$
- 10: **end for**
- 11: **return** $\mathcal{L}_g, \mathcal{L}$

In Lines 4-9, we select local landmarks corresponding to each global landmark in order to compute the topological features local to each global landmark. A node u that is not a global landmark must be in the cover of some landmark node $l \in \mathcal{L}_g$. We say u is a witness node to the node l . We assume the local topological signature does not change inside a cover. In other words, a witness node has the same topological signature as its associated landmark. That is why, instead of computing local landmarks for every node in \mathcal{V} , we compute only for the global landmarks $\mathcal{L}_g \subseteq \mathcal{V}$ (line 4). For each global landmark $l \in \mathcal{L}_g$, we construct its cover C_l in line 5 consisting of all its witness nodes. In line 6, we construct the subgraph $\mathcal{G}[C_l]$ induced by the witness nodes. Finally, in lines 7-9, we select the topmost $p\%$ of the witness nodes with the highest degrees in the induced subgraph $\mathcal{G}[C_l]$ as the local landmark for $l \in \mathcal{L}_g$.

E.1 Impact of the Number of Landmarks

It is well-known that the quality of the Witness complex-based topological features is dependent on the number of landmarks (De Silva and Carlsson 2004; Arafat, Basu, and Bressan 2019). Hence, the performance of the proposed witness topological encodings, topological loss, and, finally, the downstream classification quality is also dependent on the number of landmarks.

In order to study the accuracy and efficiency of WTGL under different numbers of landmarks, we use Algorithm 1 to select 1%, 10%, 50% nodes as landmarks, and in Figure 3, we present the accuracy and computation time of the local and global witness complex-based features on Cora-ML and Citeseer datasets. We observe that increasing the number of landmarks indeed slightly increases the accuracy, albeit with the expense of increased computation time. Due to this trade-off between accuracy and efficiency, the selection of an optimal number of landmarks is dependent on how much robustness is desired by a user within a given computation-time budget.

E.2 Comparison of WTGL and Vietoris-Rips based Topology Encoding (VRGTL)

Finally, we also observe that, on these datasets, the accuracy achieved by WTGL with 50% landmarks is close to the

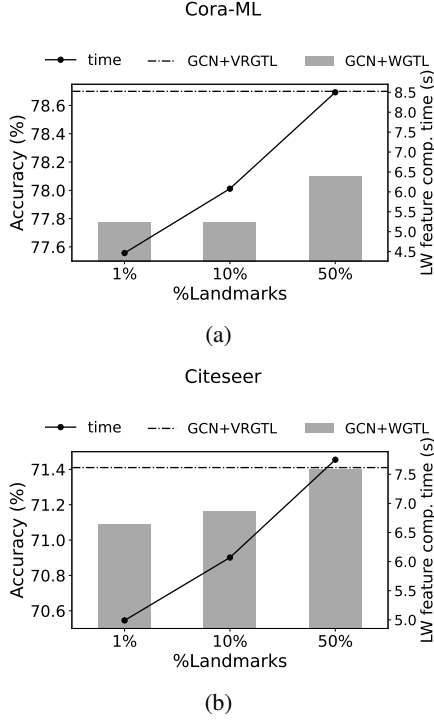


Figure 3: The trade-off between accuracy and Feature computation time of GCN+WGTL with different numbers of landmarks. The figures are under metttack with 5% perturbation rate.

	Method	Cora-ML	Citeseer
VR feature comp. time (s)	CPU (Ripser)	23286.0	1698.0
	GPU (Ripser++)	13021.5	1430.6
Witness feature comp. time (s)	Algorithm 1	8.5	7.8

Table 11: Execution times (in seconds) for computing global and local topological features. Landmark selection time is included.

accuracy achieved by adopting Vietoris-Rips-based topological feature encoding, as indicated by the dotted line representing GCN+VRGTL. A more in-depth comparison among GCN, GCN+WGTL and GCN+VRGTL is presented in Figure 3 where we compare their accuracy on Cora-ML and Citeseer under metttack. We observe that the accuracy of GCN+VRGTL is comparable to that of GCN+WGTL. These observations also highlight the flexibility of WGTL in adopting other approximate topological features.

However, computing Vietoris-Rips features is significantly more expensive than witness topological features (Arafat, Basu, and Bressan 2020). We computed Vietoris-Rips features using both CPU and GPU based state-of-the-art implementations: Ripser (Bauer 2021) and Ripser++ (Zhang, Xiao, and Wang 2020). As shown in Table 11, adopting CPU-based Vietoris-Rips PH computation into our computation pipeline incurs more than 2500x (200x) more computation time on Cora-ML (Citeseer) compared to using Witness PH computation. GPU acceleration using Ripser++ is more computation-

ally viable than CPU-based implementation yet 1500x and 180x slower than Witness feature computation on Cora-ML and Citeseer respectively.

The results demonstrate that instead of incurring 2 to 3 order of magnitude less computational time, deploying WGTL leads to similar or better accuracy to those of VRGTL across a wide range of perturbations.

F Experimental Results: WGTL against Different Attacks and Graph Structures

F.1 Performance of WGTL on targetted attack: Nettack

Dataset	Model	Number of perturbations per node		
		0	1	2
Cora-ML	GCN + GNNGuard	83.21 \pm 0.34	82.81 \pm 0.43	82.51 \pm 0.26
	GCN + GNNGuard + WGTL (ours)	84.78\pm0.43	84.25\pm0.73	83.74\pm0.96
	SimP-GCN	79.52 \pm 1.81	74.75 \pm 1.40	70.87 \pm 1.70
	SimP-GCN + WGTL (ours)	81.49\pm0.52	76.65\pm0.65	72.88\pm0.83
Citeseer	GCN + GNNGuard	71.82 \pm 0.43	71.87 \pm 0.53	71.71 \pm 0.32
	GCN + GNNGuard + WGTL (ours)	72.53\pm0.35	72.43\pm0.48	71.95\pm0.88
	SimP-GCN	73.73 \pm 1.54	73.06 \pm 2.09	72.51 \pm 1.25
	SimP-GCN + WGTL (ours)	74.32\pm0.19	74.05\pm0.71	73.09\pm0.50
Polblogs	GCN + GNNGuard	95.03 \pm 0.25	91.43 \pm 0.36	89.45 \pm 0.46
	GCN + GNNGuard + WGTL (ours)	96.22\pm0.25	91.89\pm0.57	90.35\pm0.81
	SimP-GCN	89.78 \pm 6.47	65.75 \pm 5.03	61.53 \pm 6.41
	SimP-GCN+WGTL (ours)	94.56\pm0.24	69.78\pm4.10	69.55\pm4.42

Table 12: Performances wrt existing defenses under nettack

Dataset	Model	Number of perturbations per node		
		0	1	2
Cora-ML	GCN	82.87 \pm 0.93	82.53 \pm 1.06	82.08 \pm 0.81
	GCN + WGTL (ours)	83.83\pm0.55	*83.41\pm0.87	82.74\pm0.65
	Chebnet	80.74 \pm 0.42	79.36 \pm 0.67	77.89 \pm 0.46
	Chebnet+WGTL (ours)	82.96\pm1.08	82.90\pm1.14	82.47\pm0.96
	GAT	84.25 \pm 0.67	79.88 \pm 1.09	72.63 \pm 1.56
	GAT + WGTL (ours)	*86.07\pm2.10	80.80\pm0.87	75.80\pm0.79
	GraphSAGE	81.01 \pm 0.27	80.48 \pm 0.71	80.19 \pm 0.49
	GraphSAGE + WGTL (ours)	83.63\pm0.35	83.23\pm0.21	*82.79\pm0.36
Polblogs	GCN	94.40 \pm 1.48	88.91 \pm 1.06	85.39 \pm 0.86
	GCN + WGTL (ours)	*95.95\pm0.15	*91.47\pm0.33	89.10\pm0.69
	Chebnet	73.10 \pm 7.13	65.92 \pm 5.77	63.19 \pm 5.02
	Chebnet+WGTL (ours)	92.50\pm1.10	89.33\pm0.62	88.24\pm0.64
	GAT	95.28 \pm 0.51	89.86 \pm 0.63	86.44 \pm 1.47
	GAT + WGTL (ours)	95.87\pm0.26	90.69\pm0.51	87.73\pm0.38
	GraphSAGE	94.54 \pm 0.27	90.20 \pm 0.30	89.57 \pm 0.62
	GraphSAGE + WGTL (ours)	95.58\pm0.50	90.98\pm0.27	*89.95\pm0.78

Table 13: Performance wrt GNN backbones (avg. accuracy \pm std.) under nettack

F.2 Performance of WGTL with SGC backbone

In the main paper, we have deployed WGTL with four GNN backbones: vanilla GCN, GAT, GraphSAGE and ChebNet. In order to test the versatility and flexibility of WGTL, we adopt WGTL with a more recent GNN, namely SGC (Wu et al. 2019a) as backbone. We adopt the experimental setup and landmark selection scheme described earlier in Appendix C.

Dataset	Model	Perturbation Rate		
		0%	5%	10%
Cora-ML	SGC	82.51±0.11	76.45±0.11	68.74±0.13
	SGC + WGTl (ours)	84.25±0.06	77.40±0.73	69.07±0.46
Citeseer	SGC	71.68±0.11	68.14±0.17	63.12±0.16
	SGC + WGTl (ours)	71.33±0.20	70.15±0.31	66.18±0.32
Polblogs	SGC	90.08±0.26	68.88±0.29	65.73±0.15
	SGC + WGTl (ours)	95.52±0.05	74.40±0.09	70.35±0.63

Table 14: Performance (Accuracy±Std) of SGC and SGC+WGTl under metttack.

Dataset	Model	Number of perturbations per node		
		0	1	2
Cora-ML	SGC	82.51±0.11	81.91±0.15	80.93±0.17
	SGC + WGTl (ours)	84.25±0.06	83.85±0.12	83.35±0.16
Citeseer	SGC	71.68±0.11	71.42±0.03	70.82±0.11
	SGC + WGTl (ours)	71.33±0.20	71.45±0.29	71.16±0.37
Polblogs	SGC	90.08±0.26	82.62±0.42	78.69±0.33
	SGC + WGTl (ours)	95.52±0.05	90.92±0.09	86.38±0.33

Table 15: Performance (Accuracy±Std) of SGC and SGC+WGTl under netttack.

For the attacks, we adopt the configurations and budgets as described earlier in Appendix B. Table 14 and table 15 demonstrate the performance of the backbones with and without WGTl on three representative datasets: Cora-ML, Citeseer and Polblogs, and under two different representative attacks, i.e., metttack and netttack. *We observe that incorporating WGTl improve the corresponding performance across a range of perturbation rates for both attacks.*

F.3 Performance of WGTl on other poisoning-type topological attacks: PGD and Meta-PGD

From tables 16 and 17, we observe that: (i) GCN+WGTl consistently outperforms GCN on these attacks which proves the effectiveness of our proposed WGTl, and (II) Meta-PGD is generally stronger attack than PGD for both GCN as well as GCN+WGTl.

Dataset	Model	Perturbation Rate		
		0%	5%	10%
Cora-ML	GCN	82.87±0.93	82.45±0.92	77.33±0.27
	GCN + WGTl (ours)	83.83±0.55	83.30±0.99	80.00±1.15
Citeseer	GCN	71.56±0.63	69.58±0.48	65.56±0.45
	GCN + WGTl (ours)	72.56±0.82	72.33±0.33	71.00±1.59
Pubmed	GCN	81.70±0.30	81.64±0.18	81.01±0.21
	GCN + WGTl (ours)	83.93±0.06	82.14±0.12	81.74±0.25
Polblogs	GCN	94.40±1.48	91.17±2.27	89.92±1.43
	GCN + WGTl (ours)	95.95±0.15	91.45±0.51	90.02±1.16

Table 16: Performance (Accuracy±Std) under PGD-attack.

F.4 Performance of WGTl on Heterophilic Graphs

In the previous experiments, we have used four homophilic graph datasets: Cora-ML, Citeseer, Pubmed, and Polblogs. In

Dataset	Model	Perturbation Rate		
		0%	5%	10%
Cora-ML	GCN	82.87±0.93	79.30±0.86	76.26±0.92
	GCN + WGTl (ours)	83.83±0.55	79.57±1.10	76.52±0.81
Citeseer	GCN	71.56±0.63	67.89±0.59	66.80±0.79
	GCN + WGTl (ours)	72.56±0.82	69.38±0.27	67.57±0.67
Pubmed	GCN	81.70±0.30	77.24±0.14	73.56±0.17
	GCN + WGTl (ours)	83.93±0.06	78.97±0.20	75.22±0.16
Polblogs	GCN	94.40±1.48	83.46±2.13	78.08±0.73
	GCN + WGTl (ours)	95.95±0.15	85.52±0.70	81.28±0.31

Table 17: Performance (Accuracy±Std) under Meta-PGD attack.

this section, we aim to test the performance of WGTl and its poisoned variant WGTl_P on a heterophilic graph. Adopting the same attack configurations described in Appendix B, we generate different perturbations (perturbation rates 0% to 25%) of snap-patents graph (Leskovec, Kleinberg, and Faloutsos 2005).

Heterophilic Graph Dataset. The snap-patents is a utility patent citation network. Node labels reflect the time the patent was granted, and the features are derived from the patent’s metadata. Following (Zhu et al. 2022), for better computational tractability, we sample a subset of the snap-patents data using a snowball sampling approach, where a random 20% of the neighbors for each traversed node are kept. The homophily ratio for this dataset is as low as 0.134. Hence, (Zhu et al. 2022) used this dataset as a benchmark heterophilic graph to test the robustness of many GNN architectures, including those proposed for heterophilic graphs.

Backbone GNN: H₂GCN. Recently, it has been shown that GCN and other classical GNNs (e.g. GAT) perform poorly on heterophilic graphs (Zhu et al. 2020, 2021). More recently, (Zhu et al. 2022) showed that these classical methods provide poor defence against adversarial attacks on heterophilic graphs as well. Thus, instead of GCN, we adopt H₂GCN (Zhu et al. 2020) as the backbone architecture in this experiment. H₂GCN is proposed and popularly deployed to conduct classification on the heterophilic graphs. H₂GCN proposes a set of key design techniques to improve performance of GNNs on heterophilic graphs: (1) separation of ego- and neighbor-embedding, (2) incorporation of higher-order neighborhoods, and (3) combination of intermediate representations using skip-connections.

Dataset	Models	Perturbation Rate		
		0%	5%	10%
snap-patents	GCN	26.46±0.62	25.86±1.08	25.59±0.53
	H ₂ GCN	27.71±0.86	27.55±0.19	28.62±0.38
	H ₂ GCN+WGTl (ours)	27.72±0.85	28.66±1.68	28.79±1.00
	H ₂ GCN+WGTl _P (ours)	27.72±0.85	28.02±0.38	28.72±0.76

Table 18: Performance of WGTl on a heterophilic graph: snap-patents under Metttack.

Results and Observations. For each perturbation rate, we run five experiments with H₂GCN and H₂GCN+WGTl on the corresponding perturbed snap-patents dataset, and report the mean± standard deviation of the final classification

accuracy in Table 18. The results show that H₂GCN+WGTl robustly improves the accuracy over H₂GCN by up to 4% across the perturbation rates. Note that the best-performing method APPNP (Gasteiger, Bojchevski, and Günnemann 2018)) on this dataset has been shown to have an accuracy of 27.76% under 20% perturbation (see Table 3 of Zhu et al. (2022)). Improving on that, we observe that H₂GCN+WGTl achieves 28.21% average accuracy under 20% perturbation. Exploring other heterophilic graphs, and ways of further improving the performance of WGTl on heterophilic graphs are left as a future work.

Models	Perturbation Rate	
	0%	10%
GCN	81.68 ± 0.73	71.16 ± 1.61
GCN+WGTl _P (ours)	82.62 ± 0.77	72.75 ± 1.24

Table 19: Performance of WGTl on Cora-ML under Node-feature attack using Mettack.

E.5 Performance of WGTl under attacks on node-features

We demonstrate a way to use WGTl to handle attacks on node features. We propose to feed the k -nearest neighbor graph (k -NNG) constructed from node features rather than the input graph in Figure 1. Traditionally, the k -NNG is a graph where two nodes u and v are connected by an edge if the geodesic distance $d_G(u, v)$ is among the k -th smallest distances from u to all other nodes. To handle node-feature perturbation, instead of using $d_G(u, v)$, we propose to use the cosine distance between feature vectors X_u and X_v , defined as $\left(1 - \frac{X_u \cdot X_v}{\|X_u\|_2 \|X_v\|_2}\right)$.

Table 19 presents our experimental results on the Cora-ML graph under Mettack where the cosine distance-based k NN graph has been adopted. This approach is generally effective, as the observation indicates that the GCN+WGTl_P always outperforms GCN across clean and perturbed graphs.

E.6 Performance of WGTl under adaptive adversarial attacks

Recently Mujkanovic et al. (2022) proposed to use custom adaptive attacks as a gold standard for evaluating defence methods. Hence, instead of using linearised GCN as a surrogate, we used the proposed GCN+WGTl as a surrogate to stress-test the ability of the proposed method to defend against a more powerful attack.

Adaptive Attack Settings & Baselines. The defense model WGTl, along with its hyper-parameters, is assumed to be a white box to the attacker, including the topological features on the clean graph. We do not assume that the attacker has access to the topological features on the perturbed graph because the PH topological feature computation is not differentiable; hence, it is not possible for the attacker to back-propagate gradients and compute the derivative of the adjacency matrix with respect to the features. The adaptive

Dataset	Model	Evasion Attack	Poisoning Attack
Cora-ML	GCN	60.06	60.46
	GCN+WGTl _P (ours)	60.31	63.48
	GNNGuard	61.92	60.81
	GNNGuard+WGTl _P (ours)	63.63	63.53
	GADC(IV)	72.08	73.14
Polblogs	GADC(IV)+WGTl _P (ours)	*76.16	75.65
	GCN	52.35	53.17
	GCN+WGTl _P (ours)	53.27	63.91
	GNNGuard	49.69	47.03
	GNNGuard+WGTl _P (ours)	50.41	53.58
	GADC(IV)	52.04	52.04
	GADC(IV)+WGTl _P (ours)	*87.93	54.81

Table 20: Performance from one run under PGD-based adaptive adversarial attack with 20% perturbation rate.

attack used was dubbed *Aux-attack* in the codebase of Mujkanovic et al. (2022), where they used PGD attack (Xu et al. 2019) adaptively with tanh logit margin as the attacker’s loss function.

We evaluate the effectiveness of WGTl against Aux-attack in both evasion and poisoning settings using the dataset splits from Liu et al. (2024). In the evasion attack setting, we train GCN+WGTl with clean topological features, perform Aux-attack to compute the perturbed graph, and finally, during evaluation, we plug in the topological features computed on the perturbed graph to do inference on test nodes. In the poisoning attack setting, we train GCN+WGTl (with the same architecture as the surrogate) except with the topological features computed on the poisoned graph. Hence, the target model is effectively GCN+WGTl_P in the poisoning attack setting. Finally, we evaluate the trained GCN+WGTl_P on the test nodes.

Apart from the GCN baseline, we have also tested more recently proposed two baselines in these settings: Graph adversarial diffusion convolution (GADC) (Liu et al. 2024) and GNNGuard (Zhang and Zitnik 2020).

Results and Observations. The results from one run on the Cora-ML and Polblogs dataset are presented in Table 20. The results demonstrate that our method significantly outperforms the baselines on both evasion and poisoning adaptive attack settings. For instance, it achieves up to 5.7% improvement over GADC(IV) on Cora-ML and up to 69% improvement on polblogs.

E.7 Performance of WGTl with persistence curve vectorization

Persistence curve (Chung and Lawson 2022) is a family of representations that are functions of the multiset of birth and death pairs $\{(b_i, d_i) \in \mathbb{R}^2 : d_i > b_i, \forall i \in \{1, 2, \dots, n\}\}$. Among the various functions proposed by Chung and Lawson (2022), the *Normalized life curve* has been recommended by the authors for its stability, computational efficiency, and performance. The normalized life curve is defined as the following transformation:

$$\frac{d_i - b_i}{\sum_{i=1}^n (d_i - b_i)}$$

Dataset	Models	Perturbation Rate		
		0%	5%	10%
Cora-ML	GCN	82.87 \pm 0.83	76.55 \pm 0.79	70.39 \pm 1.28
	GCN+WGTLP(PI)	83.83\pm0.55	76.96 \pm 0.76	71.31 \pm 0.85
	GCN+WGTLP(PC)	83.72 \pm 0.50	78.16\pm1.04	72.54\pm1.48
Polblogs	GCN	94.40 \pm 1.47	71.41 \pm 2.42	69.16 \pm 1.86
	GCN+WGTLP(PI)	95.95\pm0.15	73.02 \pm 1.13	74.52\pm0.28
	GCN+WGTLP(PC)	95.19 \pm 0.32	73.05\pm1.16	69.97 \pm 1.14

Table 21: Performance of WGTl with different topological vectorizations on Cora-ML under Mettack. PC = Normalized life curve, PI = Persistence image

We have replaced the persistence image vectorization in our local topology encoding (Component I) and global topology encoding (Component II) with the normalized life curve vectorization and present the accuracy on the poisoned Cora-ML and Polblogs in Table 21. We observe that on certain datasets such as Cora-ML, the persistence curve can provide slightly better robustness than the Persistence Image representations. However, the persistence curves produce a higher standard deviation than the persistence image. Since both vectorization methods produce better accuracy than the baseline, the proposed method is agnostic to the choice of alternative vectorizations of persistent topological features.